Feasibility of observing mechanical effects of cosmological neutrinos

Ignacio Ferreras
Department of Physics, Cornell University, Ithaca, New York 14853
and Center for Radiophysics and Space Research Cornell University, Ithaca, New York 14853

Ira Wasserman
Center for Radiophysics and Space Research Cornell University, Ithaca, New York 14853
and Department of Astronomy, Cornell University, Ithaca, New York 14853
(Received 17 February 1995; revised manuscript received 12 June 1995)

We reexamine mechanical effects of cosmological neutrinos, and the possibility of their detection. Classical and quantum-mechanical results are derived for the mean force on a spherical target mass due to neutrinos that are either extremely relativistic, nonrelativistic but unclustered, or nonrelativistic and clustered; results are presented for Dirac and Majorana massive neutrinos. We find that there is no $O(G_F)$ mean force, in agreement with earlier calculations. In addition, we demonstrate that there are fluctuating forces $O(G_F^2)$, which are more important than the mean force except on sufficiently long time scales that we evaluate case by case. Thus, fluctuations may act as a source of noise for any experiment seeking to detect the small, mean force due to background neutrinos even if all other sources of noise can be eliminated. In addition, we show that the fluctuating forces on a pair of nearby targets due to background neutrinos should be correlated, and that interference effects can lead to a short-range "shadowing force" between targets even in a perfectly isotropic background. Finally, the rates of phonon excitation both from the ground state and for a state with nonzero preexisting excitation are computed.

PACS number(s): 95.30.Cq, 95.35.+d, 95.55.Vj, 98.70.Vc

I. INTRODUCTION

The discovery of the cosmic microwave background radiation and its subsequent study have enabled cosmologists to model the evolution of the Universe from extremely early times to the present. The detected photons have been streaming freely since they decoupled from the rest of the cosmic plasma at a redshift $z \approx 10^3$. Thus we only have direct observational information on the state of the Universe for temperatures $T \lesssim 0.3$ eV. Any inferences about the evolution of the Universe at earlier epochs rest on additional, generally plausible physical assumptions which can only be tested indirectly [1].

If unclustered low mass or massless cosmological neutrinos could be observed, cosmologists would gain invaluable knowledge about conditions in the Universe at much higher redshifts, corresponding to $T \lesssim 1$ MeV. If clustered massive neutrinos are a major constituent of galaxies or galaxy clusters, then their discovery would shed light on the nature of cosmological dark matter. Unfortunately, the cosmological neutrinos couple to ordinary matter extremely weakly, rendering their detection exceptionally difficult.

During the past 20 years or so, several authors have investigated the possibility that mechanical effects of cosmological neutrinos on laboratory targets could be detectable. Early papers suggested that cosmological neutrinos could exert forces $O(G_F)$ on laboratory masses [2–4], but these papers were later shown to be incorrect [5–7] for reasons we review below. Subsequently, it was suggested that steady $O(G_F^2)$ forces could produce detectable effects in superconducting targets [4,8], but these suggestions have also been criticized justly [5,9,10].

Here we reexamine the problem of mechanical forces exerted by cosmological neutrinos on massive targets. One of the purposes of this paper is to investigate the competition between fluctuating and steady forces on a detector. A classical argument suffices to demonstrate why there are no steady forces $O(G_F)$ due to the neutrino background and how fluctuating forces with root-mean-square (rms) amplitudes $O(G_F)$ may arise. From the viewpoint of the target mass, the interaction energy with a sea of Dirac neutrinos is of order

$$U(\mathbf{x}_d,t) = \frac{G_F}{\mu}\int_{\mathcal{V}} d^3x\,\rho(\mathbf{x})[n_\nu(\mathbf{x}_d+\mathbf{x},t) - n_{\bar\nu}(\mathbf{x}_d+\mathbf{x},t)]\,, \tag{1.1}$$

where $\rho(\mathbf{x})$ is the mass density and μ the mass per atom of the target, and the integral is over the volume $\mathcal{V}$ of the laboratory detector, which is centered at $\mathbf{x}_d$. If $n_\nu(\mathbf{x},t)$ and $n_{\bar\nu}(\mathbf{x},t)$ are exactly uniform in space, then $U(\mathbf{x}_d,t)$ is translationally invariant,and there can be no $O(G_F)$ force on the mass. According to Eq. (1.1), the time-averaged $O(G_F)$ force on the target vanishes if the mean values of $n_\nu(\mathbf{x},t)$ and $n_{\bar\nu}(\mathbf{x},t)$ are uniform; this result may be demonstrated both classically and quantum mechanically [5–7].

Naturally occurring gradients in $n_\nu(\mathbf{x},t)$ and $n_{\bar\nu}(\mathbf{x},t)$ are expected to be insignificant; moreover, there is no known way to generate artificial density gradients large enough to result in easily measurable steady forces

$O(G_F)$ [11]. The largest naturally occurring steady forces due to the neutrino background are $O(G_F^2)$.

Equation (1.1) also suggests that density fluctuations in the neutrino (and antineutrino) background could result in nonsteady forces that are characteristically $O(G_F)$. Such forces would produce displacements of massive objects that are proportional to $t^{3/2}$ rather than t^2, which would result from constant acceleration. On sufficiently long time scales, steady forces must always produce larger displacements than nonsteady forces, but it is possible that fluctuating forces are more important on reasonable time scales for laboratory experiments. If so, fluctuating forces could be either a boon or a nuisance: They may be more readily detectable than steady forces, but also could simply provide an irreducible source of noise, frustrating the detection of steady forces. In Sec. II, we give both classical and quantum-mechanical results for the steady and fluctuating forces on a spherical scatterer. In the nonrelativistic limit, we derive results for both Dirac and Majorana neutrinos.

Neutrino density fluctuations should be correlated in space and time, with a correlation length scale $l_\nu = 1/p_\nu$ and a correlation timescale $\tau_\nu = E_\nu/p_\nu^2$, where E_ν and p_ν are the characteristic neutrino energy and momentum. For extremely relativistic background neutrinos, $E_\nu = p_\nu = T$, where $T \approx 1.95$ K is the temperature of the background, whereas for nonrelativistic background neutrinos $E_\nu = m$ and $p_\nu \approx 1.95$ K [12]; thus, for unclustered neutrinos,

$$l_\nu \approx 0.12 \text{ cm} \tag{1.2}$$

and

$$\tau_\nu \approx \begin{cases} 3.9 \times 10^{-12} \text{ s} & (m \ll T) , \\ 2.3 \times 10^{-8} m \text{ eV s} & (m \gg T) , \end{cases} \tag{1.3}$$

where $m = m$ (eV) eV. For clustered (hence nonrelativistic) neutrinos, $E_\nu = m$ and $p_\nu = m\sigma$, where $\sigma \equiv 10^{-3}\sigma_{-3}$ is the neutrino velocity dispersion; thus, for clustered neutrinos,

$$l_\nu \approx 2.0 \times 10^{-2}[m(\text{eV})\sigma_{-3}]^{-1} \text{ cm} \tag{1.4}$$

and

$$\tau_\nu \approx 6.6 \times 10^{-10}[m(\text{eV})\sigma_{-3}^2]^{-1} \text{ s} . \tag{1.5}$$

It is probably fruitless even to contemplate performing meaningful measurements of exceptionally weak forces on time scales as short as τ_ν in any of the above cases. Thus we assume below that even given a heroic experimental effort, the effects of fluctuations in the neutrino density would only be detectable on time scales $\gg \tau_\nu$. (In fact, the $t^{3/2}$ scaling of test mass displacements quoted above is valid only if $t \gg \tau_\nu$.) However, spatial correlations in the otherwise stochastic motion of a pair of test masses subject to the fluctuating forces exerted by cosmological neutrinos ought to be significant on small, but still macroscopic length scales. These correlations would be no more difficult to detect than the independent jitter of a single mass, but no easier to detect either. We consider the motion of a pair of masses in Sec. III, where we derive the two-point correlation function for spatial displacements onto time scales along compared to τ_ν. In Sec. III we also consider the effect that distortions of the wave function of a plane wave neutrino by one mass may have on the other. As we shall see, there is a kind of shadowing force between the masses even if they are immersed in a perfectly isotropic background.

Finally, it is interesting to consider whether or not excitations of internal modes of a complex system by background neutrinos may occur at a sizable rate. In Sec. IV, we calculate the rate of phonon production in an atomic lattice by interactions with cosmological neutrinos. As we shall see, the rate of single-phonon excitations from the ground state is miniscule for any given mode, although the net rate of phonon production (that is, production rate minus destruction rate) for an already excited solid may be larger.

A summary of the basic results of our paper and a discussion of their implications may be found in Sec. V. The bottom line may be stated succinctly: We identify no new and promising schemes for detecting cosmological neutrinos, but we may have found reasons for additional skepticism among those who hope that these elusive particles may someday be observed. In this section, we briefly discuss the implications of the standard quantum limit on displacement measurements for the prospects of detecting mechanical effects of cosmological neutrinos. We do not discuss possible quantum nondemolition measurements, except to note that the familiar treatments (in the context, for example, of measuring small displacements of target masses by gravitational waves) are not strictly applicable, since they consider the limitations on determining the effects of classical forces on a quantum system; forces exerted by the neutrino background cannot be modeled in this way.

Throughout this paper, we adopt units in which $\hbar = c = k = 1$. However, on the occasion we give velocities in km s^{-1}, temperatures in K, etc., where doing so is appropriate. We also convert all observationally interesting quantities to conventional units; e.g., time scales are given in seconds, days, months, or years.

II. STEADY AND NONSTEADY FORCES

A. Classical calculation

Consider a sphere of radius R within which neutrinos experience a uniform potential V surrounded by a vacuum, where the potential vanishes. Focus first on neutrinos incident on the sphere with momentum $\mathbf{p}$ at any impact parameter $\mathbf{b}$ relative to a path that cuts through the center of the sphere. Upon entering the sphere, each neutrino is deflected by a radially directed (δ-function) force. As a result, the radially directed component of neutrino momentum is changed from $p_r = -p(1 - b^2/R^2)^{1/2}$ (where $b = |\mathbf{b}|$) to

$$p_r' = p_r\sqrt{Q} , \tag{2.1}$$

where, to all orders in V,

$$Q \equiv 1 - \frac{2EV - V^2}{p_r^2} \tag{2.2}$$

for a neutrino energy $E = (p^2 + m^2)^{1/2}$. Only positive values of Q are permitted classically; if $V > 0$ (as it is, for example, for neutrinos incident on ordinary matter), then Q may be negative for small enough values of p_r. Requiring $Q > 0$ is equivalent to

$$1 - \frac{b^2}{R^2} > \frac{2EV - V^2}{p^2} \approx \frac{2EV}{p^2} , \tag{2.3}$$

which constitutes a classical impact parameter limit. We return to this point later in this subsection.

It is straightforward to use Eq. (2.1) and the continuity of the nonradial neutrino momentum across the boundary of the sphere to compute the classical path taken by the neutrino within the sphere. Given this path, the point at which the neutrino emerges from the sphere can be determined easily. At this point, the neutrino experiences a second deflection; overall, the net change in neutrino momentum is

$$\frac{\Delta\mathbf{p}}{p} = \frac{2\mathbf{b}(1-\sqrt{Q})(1-b^2/R^2)^{1/2}[1+(1-b^2/R^2)(\sqrt{Q}-1)]}{R[1+(1-b^2/R^2)(Q-1)]} - \frac{2\hat{\mathbf{p}}(1-\sqrt{Q})^2(b^2/R^2)(1-b^2/R^2)}{1+(1-b^2/R^2)(Q-1)} ; \tag{2.4}$$

when Q is close to one, Eq. (2.4) reduces to

$$\frac{\Delta\mathbf{p}}{p} \approx \frac{2\mathbf{b}}{R}\left(1-\frac{b^2}{R^2}\right)^{1/2}(1-\sqrt{Q}) - 2\hat{\mathbf{p}}\frac{b^2}{R^2}\left(1-\frac{b^2}{R^2}\right)(1-\sqrt{Q})^2 . \tag{2.5}$$

Individual neutrinos passing through the sphere give it sideways impulses $\propto 1-\sqrt{Q} \approx EV/p_r^2$, but these average to zero for a uniform beam, which samples all impact parameters equally [13]. The lowest-order mean force is due to the parallel component of the impulse, which is $\propto (1-\sqrt{Q})^2 \approx E^2V^2/p_r^4$. Integrating $\Delta\mathbf{p}$ over impact parameters gives ($x = b/R$)

$$\int d^2b\,\Delta\mathbf{p} \approx -\hat{\mathbf{p}}\frac{4\pi R^2E^2V^2}{p^3}\int_0^1 \frac{dx\,x^3}{1-x^2} , \tag{2.6}$$

which diverges logarithmically at impact parameters $b/R \to 1$. Cutting off the integral at $1 - b/R = \epsilon$, we get

$$\int d^2b\,\Delta\mathbf{p} \approx -\hat{\mathbf{p}}\frac{2\pi R^2E^2V^2}{p^3}\ln(1/\epsilon) . \tag{2.7}$$

There are two possible choices for ϵ. The first is the classical cutoff implicit in Eq. (2.3); i.e., for $V \ll 1$, $\epsilon \approx EV/p^2$. The second is a quantum cutoff: On length scales smaller than the de Broglie wavelength, $1/p$, the wavelike nature of the incident neutrino cannot be ignored. Thus we get

$$\epsilon = \begin{cases} EV/p^2, & EVR/p \gg 1 \ \text{(classical)} , \\ 1/pR, & EVR/p \ll 1 \ \text{(quantum)} . \end{cases} \tag{2.8}$$

The condition $EVR/p \ll 1$ is just the condition for validity of the Born approximation in a quantum-mechanical calculation of the deflection. In all cases of interest, this will be satisfied easily, and the quantum cutoff is the correct choice [14].

Fluctuations in the force experienced by a sphere bombarded by neutrinos will be determined by the mean-square impulse imparted in a time t. In order to calculate the fluctuations, we shall need ($x = b/R$)

$$\int d^2b|\Delta\mathbf{p}|^2 \approx \frac{8\pi R^2E^2V^2}{p^2}\int_0^1 \frac{dx\,x^3}{1-x^2} \approx \frac{4\pi R^2E^2V^2}{p^2}\ln(1/\epsilon) . \tag{2.9}$$

This integral diverges logarithmically in exactly the same way as Eq. (2.6), and we have introduced an identical impact parameter cutoff.

The mean force experienced by the sphere is found by integrating Eq. (2.6) over the flux of incident neutrinos. We shall assume that V is independent of neutrino momentum, which is correct for Dirac neutrinos and antineutrinos. Let $N_\mathbf{p}$ be the occupation number for states of momentum $\mathbf{p}$; then, the mean force is

$$\mathbf{F} \approx \frac{2\pi R^2V^2}{(2\pi)^3}\int d^3p\frac{E\mathbf{p}}{p^3}N_\mathbf{p}\ln(1/\epsilon) . \tag{2.10}$$

For extremely relativistic neutrinos,

$$\mathbf{F} \approx \frac{2\pi R^2V^2}{(2\pi)^3}\int d^3p\frac{\mathbf{p}}{p^2}N_\mathbf{p}\ln(1/\epsilon) , \tag{2.11}$$

whereas for nonrelativistic neutrinos

$$\mathbf{F} \approx \frac{2\pi R^2V^2m}{(2\pi)^3}\int d^3p\frac{\mathbf{p}}{p^3}N_\mathbf{p}\ln(1/\epsilon) . \tag{2.12}$$

In the last two equations, we have ignored Fermi suppression, consistent with the spirit of a classical calculation. We include this effect, which is due to the nonzero occupation of neutrino final states, in our quantum-mechanical treatment [cf. Eq. (2.28)], although it turns out to vanish for elastic scattering (see Sec. II B 1).

We are interested in neutrino distributions which are isotropic in a frame of reference moving relative to the deflecting sphere at a velocity $-\mathbf{v}$. For both relativistic and nonrelativistic neutrinos, the integrals are most easily done in the isotropic frame. Consider the relativistic case first. Here it is easiest to use the Lorentz invariance of d^3p/p and $N_\mathbf{p}$ to effect the transformation; substituting in addition the relation

$$\frac{\mathbf{p}}{p} = \frac{\mathbf{p}'}{p'} - \mathbf{v} + \frac{\mathbf{p}'\cdot\mathbf{v}\mathbf{p}'}{p'} , \tag{2.13}$$

which is valid for $|\mathbf{v}| \ll 1$, we find

$$\mathbf{F} \approx -\frac{2R^2V^2}{3\pi}\mathbf{v}\int_0^\infty dp'\,p'N_{p'}\ln(1/\epsilon)\ . \tag{2.14}$$

Substituting $N_p = [\exp(p/T)+1]^{-1}$, the appropriate occupation number for background neutrinos, and approximating $\ln(1/\epsilon) \approx \ln(RT)$, we find

$$\mathbf{F} \approx -\frac{\pi R^2V^2T^2\ln(RT)}{18}\mathbf{v}\ . \tag{2.15}$$

For nonrelativistic neutrinos,

$$\mathbf{F} \approx \frac{2\pi R^2V^2m}{(2\pi)^3}\int d^3p'\,N_{p'}\frac{\mathbf{p}'-\mathbf{p}_0}{|\mathbf{p}'-\mathbf{p}_0|^3}\ln(|\mathbf{p}'-\mathbf{p}_0|R)\ , \tag{2.16}$$

using the Born approximation for ϵ, where $\mathbf{p}_0 = m\mathbf{v}$. We can get a rough approximation to the integral by pulling the logarithmic factor out of the integrand and replacing it by a typical value $\ln\Lambda$; doing so gives

$$\mathbf{F} \approx -\frac{R^2V^2m\ln\Lambda}{\pi}\frac{\mathbf{p}_0}{p_0^3}\int_0^{p_0} dp\,p^2N_p\ . \tag{2.17}$$

It is straightforward to verify from Eq. (2.16) directly that Eq. (2.17) is a good approximation when p_0 is either large or small compared to $\bar{p}$, a typical neutrino momentum in the isotropic frame, provided that we choose $\Lambda \sim p_0R$ when $p_0 \gg \bar{p}$ and $\Lambda \sim \bar{p}R$ when $p_0 \ll \bar{p}$. For unclustered, nonrelativistic neutrinos, $N_p = [\exp(p/T)+1]^{-1}$, just as for relativistic neutrinos, and we find

$$\mathbf{F} \approx -\frac{R^2V^2T^3m\ln\Lambda}{\pi}\frac{\mathbf{p}_0}{p_0^3}\int_0^{p_0/T}\frac{dx\,x^2}{e^x+1} \approx \begin{cases} -[R^2V^2m^2\ln(RT)/6\pi]\mathbf{v} & (m \ll T/v)\ , \\ -[3\zeta(3)R^2V^2T^3\ln(mvR)/2\pi mv^3]\mathbf{v} & (m \gg T/v)\ , \end{cases} \tag{2.18}$$

using $v \approx 370\ \mathrm{km\,s^{-1}}$, $T/v \approx 0.14$ eV [15]. For clustered neutrinos, let us adopt $N_p = N_0\exp(-p^2/2m^2\sigma^2)$ and assume a mean neutrino velocity $\mathbf{v}$ relative to the laboratory (with $v \equiv |\mathbf{v}|$). We then find

$$\mathbf{F} \approx -\frac{N_0R^2V^2m^2\sigma^3\ln\Lambda}{\pi v^3}\Phi_D\left(\frac{v}{\sqrt{2}\sigma}\right)\mathbf{v}\ , \tag{2.19}$$

where

$$\Phi_D(z) = -\sqrt{2}ze^{-z^2} + \sqrt{\pi/2}\,\mathrm{erf}(z) \approx \begin{cases} 2\sqrt{2}z^3/3 & (z \ll 1)\ , \\ 0.5359 & (z = 1)\ , \\ \sqrt{\pi/2} & (z \gg 1)\ . \end{cases} \tag{2.20}$$

Practically speaking, we expect $v/\sqrt{2}\sigma \approx 1$ for neutrinos clustered in the galactic halo and $v/\sqrt{2}\sigma \sim 1$ for neutrinos in the local supercluster. Thus, in all cases, we may choose $\Lambda \sim m\sigma R \sim mvR$ for clustered neutrinos.

In more or less the same fashion, the growth rate of momentum fluctuations, dp^2/dt, may be evaluated by integrating Eq. (2.9) over the flux of incident neutrinos; we find

$$\frac{dp^2}{dt} \approx \frac{4\pi R^2V^2}{(2\pi)^3}\int d^3p\frac{E}{p}N_{\mathbf{p}}\ln(1/\epsilon)\ , \tag{2.21}$$

where we have ignored Fermi suppression once again in this classical calculation of the fluctuations [cf. Eq. (2.29)]. Equation (2.21) becomes

$$\frac{dp^2}{dt} \approx \frac{4\pi R^2V^2}{(2\pi)^3}\int d^3p\,N_{\mathbf{p}}\ln(1/\epsilon) \approx \frac{3\zeta(3)R^2V^2T^3\ln(RT)}{\pi} \tag{2.22}$$

for extremely relativistic neutrinos and

$$\frac{dp^2}{dt} \approx \frac{4\pi R^2V^2m}{(2\pi)^3}\int\frac{d^3p}{p}N_{\mathbf{p}}\ln(1/\epsilon) \approx \frac{4\pi R^2V^2m\ln\Lambda}{(2\pi)^3}\int d^3p'\frac{N_{p'}}{|\mathbf{p}'-\mathbf{p}_0|} \tag{2.23}$$

for nonrelativistic neutrinos, where $\Lambda \sim p_0R$ for $p_0 \gg \bar{p}$ and $\Lambda \sim \bar{p}R$ for $p_0 \ll \bar{p}$. For unclustered massive neutrinos, Eq. (2.23) gives

$$\frac{dp^2}{dt} \approx \begin{cases} \pi R^2V^2T^2m\ln(RT)/6 & (m \ll T/v)\ , \\ 3\zeta(3)R^2V^2T^3\ln(mvR)/\pi v & (m \gg T/v)\ , \end{cases} \tag{2.24}$$

and, for clustered massive neutrinos,

$$\frac{dp^2}{dt} \approx \sqrt{2/\pi}\frac{N_0R^2V^2m^3\sigma^3\ln\Lambda}{v}\mathrm{erf}\left(\frac{v}{\sqrt{2}\sigma}\right)\ , \tag{2.25}$$

where $\Lambda \sim mvR \sim m\sigma R$.

Implicit in a classical derivation of forces exerted on a target sphere by background neutrinos is the assumption that the typical neutrino momentum $p_\nu \gg 1/R$. Since both $\mathbf{F}$ and dp^2/dt increase $\propto R^2\ln(p_\nu R)$, the acceleration of the sphere decreases with radius $\propto R^{-1}\ln(p_\nu R)$ and its variance decreases even more rapidly, $\propto R^{-4}\ln(p_\nu R)$. Ultimately, mechanical measurements of weak forces involve determining accelerations of test masses; the classical arguments given above suggest that smaller masses are subject to larger accelerations. For very small target masses $R \lesssim 1/p_\nu$, the classical arguments are no longer valid, and a quantum-mechanical treatment is needed to evaluate the test particle motion. As we shall see, both $\mathbf{F}$ and dp^2/dt increase with size for $R \lesssim p_\nu^{-1}$, and the acceleration and its variance peak at $R \sim p_\nu^{-1}$.

B. Quantum-mechanical treatment: Born approximation

The Lagrangian density for the interaction of neutrinos with a classical source is [16]

$$\mathcal{L} = -\frac{G_F}{\sqrt{2}} j^\lambda(x)\bar{\nu}\gamma_\lambda(1+\gamma_5)\nu \ , \tag{2.26}$$

where, in the rest frame of the source, $j^0(x) = C_V\rho(\mathbf{x})/\mu$, assuming an unpolarized target, $\rho(\mathbf{x})$ is the mass density, and $\mu = Am_p$ is the mass per atom of the target. The vector coupling constant

$$C_V = \begin{cases} (3Z-A)/2 & \text{for } \nu_e \ , \\ (Z-A)/2 & \text{for } \nu_\mu \text{ and } \nu_\tau \ , \end{cases} \tag{2.27}$$

where Z is the number of protons or electrons per particle in the target [17]. Using this model for the interaction of neutrinos with the target mass, we find

$$\mathbf{F} = \frac{G_F^2M^2}{\mu^2(2\pi)^5}\int \frac{d^3p_i}{E_i}\frac{d^3p_f}{E_f}\delta(E_f-E_i)(\mathbf{p}_i-\mathbf{p}_f)|W_V(|\mathbf{p}_i-\mathbf{p}_f|R)|^2N_{\mathbf{p}_i}(1-N_{\mathbf{p}_f})G_\nu(\mathbf{p}_i,\mathbf{p}_f) \tag{2.28}$$

and

$$\frac{dp^2}{dt} = \frac{G_F^2M^2}{\mu^2(2\pi)^5}\int \frac{d^3p_i}{E_i}\frac{d^3p_f}{E_f}\delta(E_f-E_i)|\mathbf{p}_i-\mathbf{p}_f|^2|W_V(|\mathbf{p}_i-\mathbf{p}_f|R)|^2N_{\mathbf{p}_i}(1-N_{\mathbf{p}_f})G_\nu(\mathbf{p}_i,\mathbf{p}_f) \ , \tag{2.29}$$

where $M = 4\pi\rho R^3/3$ is the mass of the (uniformly dense) target,

$$W_V(z) = C_VW(z) = \frac{3C_V(\sin z - z\cos z)}{z^3} \ . \tag{2.30}$$

$N_{\mathbf{p}_i}$ and $N_{\mathbf{p}_f}$ are initial and final state occupation numbers, and

$$G_\nu(\mathbf{p}_i,\mathbf{p}_f) = \begin{cases} p_ip_f + \mathbf{p}_i\cdot\mathbf{p}_f & \text{(Majorana and extremely relativistic Dirac)} \ , \\ m^2/2 & \text{(nonrelativistic Dirac)} \ . \end{cases} \tag{2.31}$$

Note that in the nonrelativistic limit, $\mathbf{F}$ and dp^2/dt will not be strictly zero for scattering of Majorana particles by an unpolarized target, but will be smaller than their values for Dirac particles by a factor $\sim p_\nu^2/m^2$. For scattering of nonrelativistic Majorana neutrinos by a polarized target of mean electron spin $\langle\mathbf{s}_e\rangle$, we can use the results derived below for scattering of nonrelativistic Dirac neutrinos by an unpolarized target if we make the substitution $C_V^2 \to Z^2|\langle\mathbf{s}_e\rangle|^2$.

1. Mean force

The correction for Fermi suppression vanishes for the mean force $\mathbf{F}$; this may be seen most easily by noting that the terms responsible for Fermi suppression in the integrand of Eq. (2.28) are antisymmetric upon interchange of initial and final states. We then find

$$\mathbf{F} = \frac{G_F^2C_V^2M^2}{2\mu^2(2\pi)^4}\int d^3p\frac{\mathbf{p}}{Ep^3}N_{\mathbf{p}}\int_0^{2p} dq\, q^3W^2(qR)\tilde{G}(p,q) \ , \tag{2.32}$$

where

$$\tilde{G}(p,q) = \begin{cases} 2p^2 - q^2/2 & \text{(Majorana and extremely relativistic Dirac} \\ m^2/2 & \text{(nonrelativistic Dirac)} \ . \end{cases} \tag{2.33}$$

For large R, the inner integral is approximately $\frac{9}{2}R^{-4}\tilde{G}(p,0)\ln(2pR)$, and we find

$$\mathbf{F} \approx \frac{G_F^2C_V^2\rho^2R^2}{4\pi^2\mu^2}\int d^3p\frac{\mathbf{p}}{Ep^3}N_{\mathbf{p}}\tilde{G}(p,0)\ln(2pR) \ . \tag{2.34}$$

Equation (2.34) is equivalent to Eqs. (2.11) and (2.12) for Dirac neutrinos if we identify

$$|V| = \begin{cases} G_FC_V\rho\sqrt{2}/\mu & \text{(relativistic Dirac)} \ , \\ G_FC_V\rho/\sqrt{2}\mu & \text{(nonrelativistic Dirac)} \ , \end{cases} \tag{2.35}$$

which are the same as the well-known results derived from forward scattering amplitudes, as they should be, since scattering from a large target is dominated by momentum transfers $\sim R^{-1}$, which is small. These substitutions are not valid, of course, for Majorana neutrinos.

Analytic results for the mean force may be found in various limits. In general, the accelerations due to Dirac neutrinos are of the form

$$\mathbf{a} = \frac{G_F^2C_V^2\rho}{\mu^2v_\nu^2}\mathbf{S}_\nu\mathcal{F}_D(\hat{R}) \ , \tag{2.36}$$

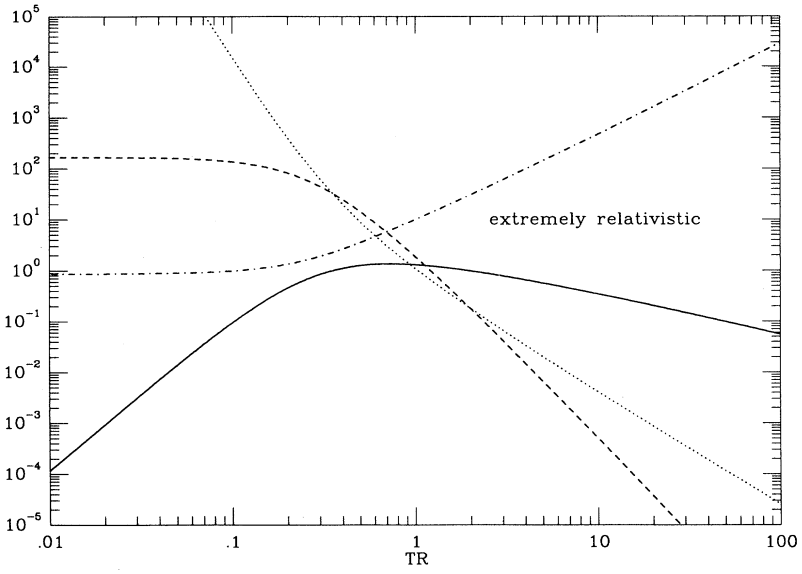

FIG. 1. Dimensionless acceleration [$\mathcal{F}_D(\hat{R})$, solid line], fluctuation [$\mathcal{G}_D(\hat{R})$, dashed line], time scale [$\mathcal{T}_D(\hat{R}) = \mathcal{G}_D(\hat{R})/\mathcal{F}_D^2(\hat{R})$, dotted line], and scattering rate [$\mathcal{R}_D(\hat{R})\mathcal{T}_D(\hat{R})$, dot-dashed line] for extremely relativistic neutrinos. The dimensionless radius $\hat{R} = TR$ in this case.

where $\mathbf{S}_\nu = n_\nu \mathbf{v}$ is the neutrino flux (with n_ν the neutrino number density), v_ν is the typical neutrino speed, $\hat{R} = p_\nu R$, and $\mathcal{F}_D(\hat{R}) \sim \hat{R}^3$ for $\hat{R} \lesssim 1$ and $\mathcal{F}_D(\hat{R}) \sim \hat{R}^{-1} \ln \hat{R}$ for $\hat{R} \gtrsim 1$; for Majorana neutrinos, the acceleration is always of the form

$$\mathbf{a} = \frac{G_F^2 C_V^2}{\mu^2} \mathbf{S}_\nu \mathcal{F}_M(\hat{R}) \ , \tag{2.37}$$

where $\mathcal{F}_M(\hat{R})$ has limiting behavior similar to $\mathcal{F}_D(\hat{R})$. The peak acceleration is at $\hat{R} \sim 1$ or $R \sim p_\nu^{-1}$.

The solid lines in Figs. 1–4 show the results of evaluating $\mathcal{F}_D(\hat{R})$, and the solid lines in Figs. 5–7 show the results of evaluating $\mathcal{F}_M(\hat{R})$ directly from Eq. (2.32). For clustered Dirac or Majorana neutrinos, we have only evaluated the integrals for $v = \sqrt{2}\sigma$, which would be appropriate for neutrinos clustered in the galaxy in a nonrotating halo. It is easy to extend the calculations to any value of v/σ. Table I summarizes the appropriate choices for v_ν, E_ν, and p_ν for the various cases, and Table II evaluates the characteristic acceleration, that is, the magnitude of the factor multiplying $\mathcal{F}_D(\hat{R})$ or $\mathcal{F}_M(\hat{R})$, whichever is appropriate.

2. *Fluctuations*

Fluctuating forces may be evaluated from Eq. (2.29) in much the same fashion as the mean forces were evaluated from Eq. (2.28). Although the correction for Fermi suppression in dp^2/dt does not vanish in general, as it did in the evaluation of $\mathbf{F}$, it is only significant when the magnitude of the mean neutrino momentum, $\sim E_\nu \mathbf{v}$, is $\lesssim \bar{p}$, the characteristic neutrino momentum in the isotropic

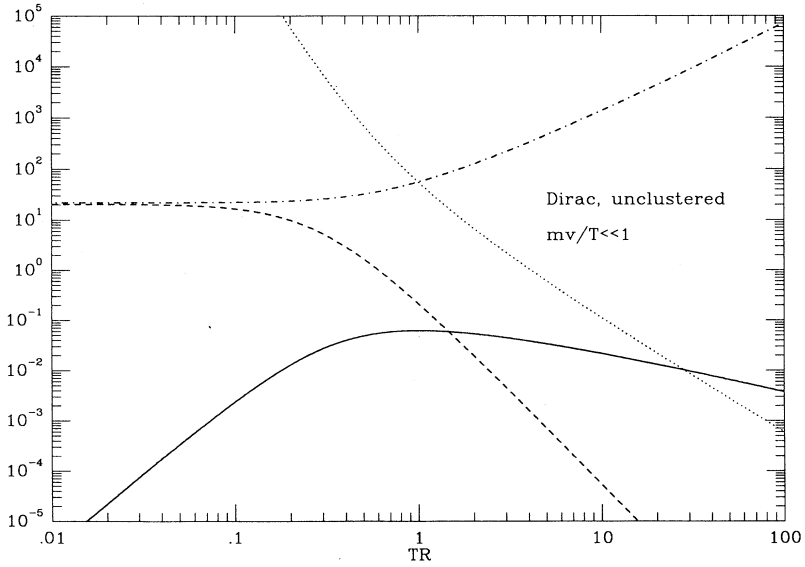

FIG. 2. Same as Fig. 1, except for unclustered, nonrelativistic Dirac neutrinos with $mv \ll T$. The dimensionless radius is $\hat{R} = TR$ in this case, too.

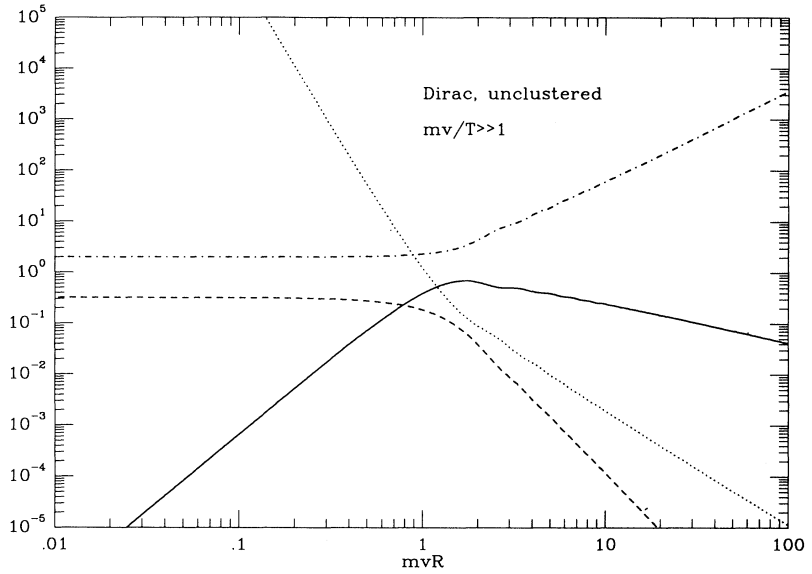

FIG. 3. Same as Fig. 1, except for unclustered, nonrelativistic Dirac neutrinos with $mv \gg T$. The dimensionless radius is $\hat{R} = mvR$ in this case.

frame. Thus we include Fermi suppression when calculating dp^2/dt for massless neutrinos and for unclustered massive neutrinos with $m \ll T/v$; we omit it for unclustered neutrinos with $m \gg v$. [18] We also ignore Fermi suppression for clustered neutrinos, but for a different reason: The neutrino distribution function we have adopted in that case is schematic and is only valid up to $O(N_0)$.

The quantity

$$\frac{dv^2}{dt} \equiv M^{-2}\frac{dp^2}{dt} \tag{2.38}$$

is independent of R at small R and decreases $\propto R^{-4}\ln(p_\nu R)$ at large R. In general, for Dirac neutrinos,

$$\frac{dv^2}{dt} = \frac{G_F^2 C_V^2 E_\nu^2 p_\nu^2 n_\nu v_\nu}{\mu^2}\mathcal{G}_D(\hat{R}) , \tag{2.39}$$

where $\mathcal{G}_D(\hat{R}) = \text{const}$ for $\hat{R} \lesssim 1$ and $\mathcal{G}_D(\hat{R}) \sim \hat{R}^{-4}\ln\hat{R}$ for $\hat{R} \gtrsim 1$; for Majorana neutrinos,

$$\frac{dv^2}{dt} = \frac{G_F^2 C_V^2 p_\nu^4 n_\nu v_\nu}{\mu^2}\mathcal{G}_M(\hat{R}) , \tag{2.40}$$

where $\mathcal{G}_M(\hat{R})$ has limiting behavior similar to that of $\mathcal{G}_D(\hat{R})$. The dashed lines in Figs. 1–7 show the results of numerical evaluation of $\mathcal{G}_D(\hat{R})$ or $\mathcal{G}_M(\hat{R})$, whichever is appropriate, for the various cases of interest. Table II also gives numerical values for the characteristic values of dv^2/dt.

A free target mass suspended in otherwise empty space will approach the thermal speed $v_{\rm th} = \sqrt{3T/M}$, as a result of its interaction with a thermal bath of light particles at temperature T. When equilibrium is attained,

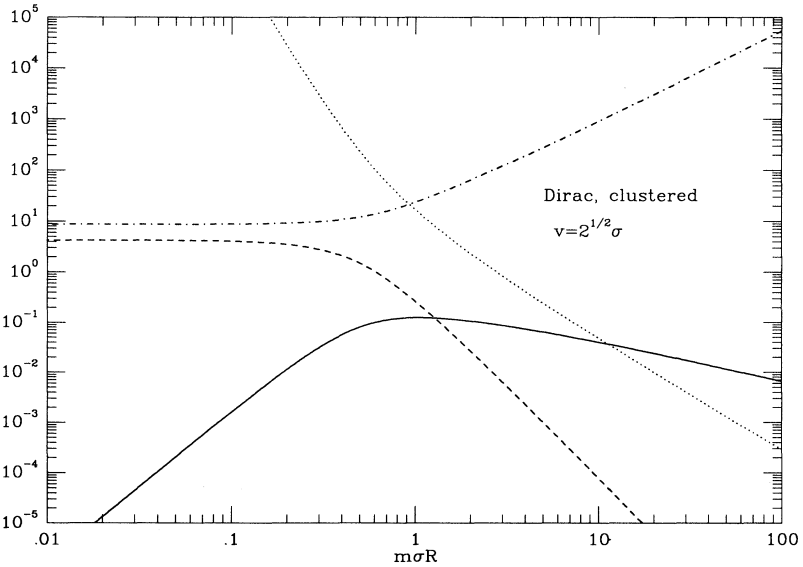

FIG. 4. Same as Fig. 1, except for clustered Dirac neutrinos with $v = 2^{1/2}\sigma$. The dimensionless radius is $m\sigma R$ in this case.

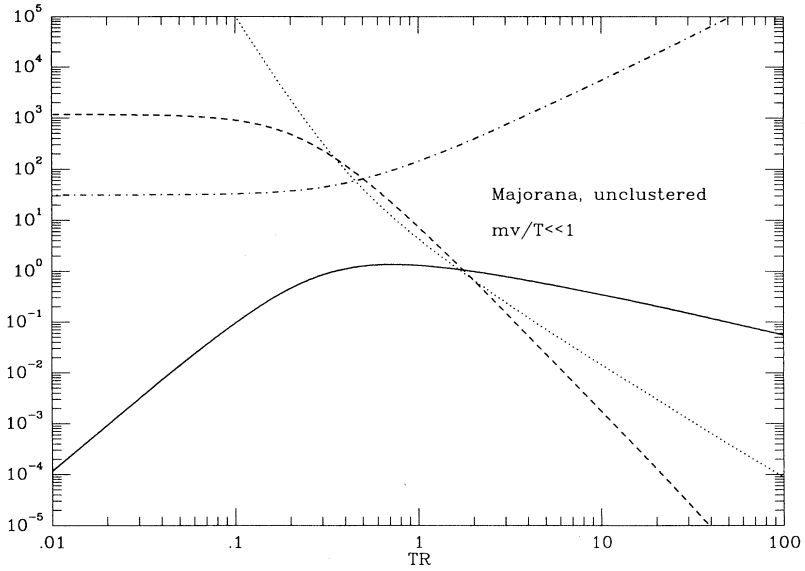

FIG. 5. Analogue of Fig. 2, but for Majorana neutrinos.

$$\left\langle \mathbf{F}\cdot\mathbf{v}+\frac{1}{2M}\frac{dp^2}{dt}\right\rangle = 0\ , \tag{2.41}$$

which means that the average work done on an ensemble of identical target masses is zero. It is straightforward to verify that Eq. (2.41) is indeed satisfied for either extremely relativistic neutrinos or clustered neutrinos (with $T = m\sigma^2$). (In general, $v_{\rm th} \ll v_\nu$, and so the low-velocity limit must be employed to verify this result for clustered neutrinos.) Strict thermal equilibrium can never be attained by free target masses interacting with unclustered massive neutrinos, which are well out of thermal equilibrium themselves. In any case, thermal equilibrium with the neutrino background is of no practical importance for two reasons. First, the relaxation time scale $t_{\rm th}$ for a free target mass in empty space is enormously long: For $\hat{R} \sim 1$, $t_{\rm th} \sim \mu^2 v_\nu^2/n_\nu G_F^2 C_V^2 \rho$ for Dirac neutrinos and a factor $\sim v_\nu^{-2}$ longer for Majorana neutrinos; numerically, $t_{\rm th} \sim 10^{34}$ yr for extremely relativistic neutrinos, $t_{\rm th} \sim 10^{23}$ yr for clustered Dirac neutrinos, and $t_{\rm th} \sim 10^{29}$ yr for clustered Majorana neutrinos. Second, target masses in the laboratory are not free and are constrained to move with the Earth through the background neutrinos at a typical speed $\sim 10^{-3}c$.

C. Mean forces vs fluctuations

Consider an ideal experiment in which all sources of acceleration except forces due to the neutrino background have been eliminated. Then, in a time interval t, the mean force acting on a target mass produces a directed momentum $\mathbf{F}t$, and the fluctuating forces acting on it produce a randomly oriented momentum of typical mag-

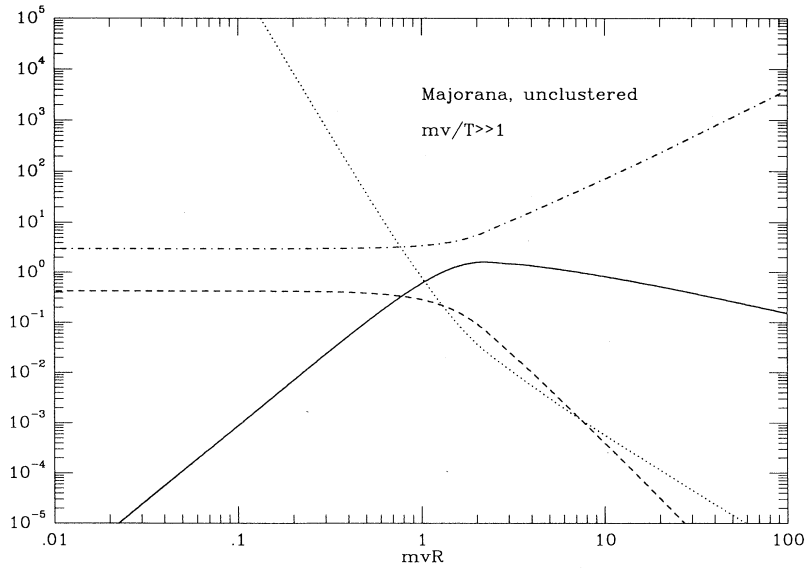

FIG. 6. Analogue of Fig. 3, but for Majorana neutrinos.

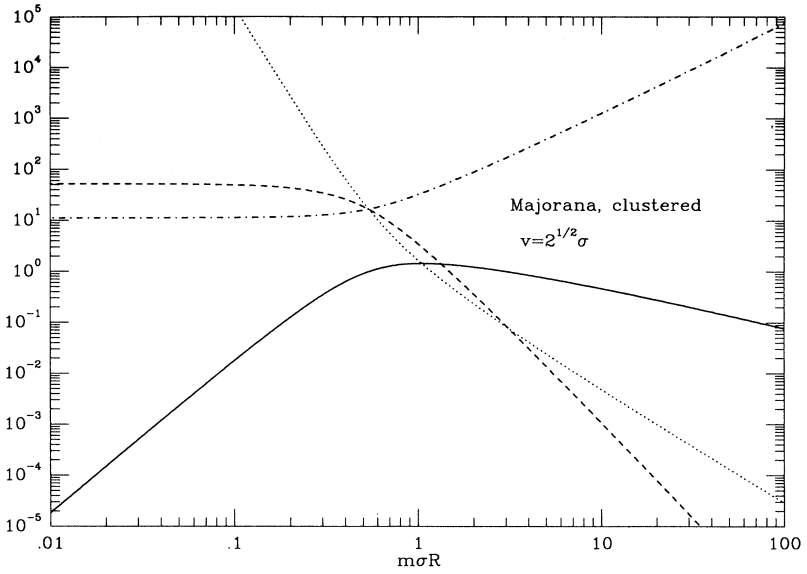

FIG. 7. Analogue of Fig. 4, but for Majorana neutrinos.

nitude $\sqrt{t\,dp^2/dt}$. Clearly, the fluctuations are more important at early times, and the mean force is more important at late times. The critical time t_c at which the integrated impulses have the same order of magnitude is

$$t_c = \frac{dp^2/dt}{|\mathbf{F}|^2} \ . \tag{2.42}$$

An experiment expressly designed to pick out the directed force due to the neutrino background must run for a time $\gtrsim (S/N)^2 t_c$ in order to distinguish the signal due to $\mathbf{F}$ from the noise due to dp^2/dt at a level S/N. For Dirac neutrinos,

$$t_c = \frac{E_\nu^2 p_\nu^2 v_\nu^5 \mu^2}{G_F^2 C_V^2 \rho^2 n_\nu |\mathbf{v}|^2} \mathcal{T}_D(\hat{R}) \ , \tag{2.43}$$

where $\mathcal{T}_D(\hat{R}) = \mathcal{G}_D(\hat{R})/\mathcal{F}_D^2(\hat{R})$, and for Majorana neutrinos,

$$t_c = \frac{p_\nu^4 v_\nu \mu^2}{G_F^2 C_V^2 \rho^2 n_\nu |\mathbf{v}|^2} \mathcal{T}_M(\hat{R}) \ , \tag{2.44}$$

where $\mathcal{T}_M(\hat{R}) = \mathcal{G}_M(\hat{R})/\mathcal{F}_M^2(\hat{R})$; generally speaking, t_c is a factor $\sim v_\nu^{-2}$ longer for Majorana neutrinos than it is for Dirac neutrinos. The dotted lines in Figs. 1–7 show the results of evaluating $\mathcal{T}_D(\hat{R})$ and $\mathcal{T}_M(\hat{R})$. The characteristic time scale t_c can be surprisingly long. At $\hat{R} \sim 1$, where accelerations are largest, we find t_c ~days for unclustered Dirac neutrinos with $mv/T \sim 1$, t_c ~months for Dirac neutrinos clustered in the galaxy, $t_c \sim 10^4$ yr for unclustered Majorana neutrinos with $mv/T \sim 1$, $t_c \sim 10^5$ yr for Majorana neutrinos clustered in the galaxy, and $t_c \sim 10^7$ yr for extremely relativistic neutrinos.

Undeniably, the detection of dynamical effects due to neutrinos or any other cosmological background would be facilitated by a foreknowledge of the direction of the force exerted and of its time dependence. For unclustered neutrinos, the direction of $\mathbf{F}$ is set by the direction of motion of the Earth relative to the cosmic microwave background. The direction of our peculiar velocity varies in the course of a year and is relatively well known. The direction of our relative motion with respect to neutrinos clustered in the galactic halo or local supercluster is less well known, but should also vary over the course of a year. The fluctuating forces should not vary systematically with time to the same extent, although the fluctuation tensor $d(p_i p_j)/dt$ ought to reflect, to varying degrees in the different cases, a preferred axis along $\mathbf{v}$.

TABLE I. Energies, momenta, and speeds.

Case	E_ν	p_ν	v_ν
Relativistic	$T = 1.95$ K	$T = 1.95$ K[a]	1
Dirac, unclustered	$m \ll T/v$	$T = 1.95$ K	T/m
Dirac, unclustered	$m \gg T/v$	mv	$v = 10^{-3} v_{-3}$[b]
Dirac, clustered	$m = 10 m_{10}$ eV	$m\sigma$	$\sigma = 10^{-3}\sigma_{-3}$
Majorana, unclustered	$m \ll T/v$	$T = 1.95$ K	T/m
Majorana, unclustered	$m \gg T/v$	mv	$v = 10^{-3} v_{-3}$
Majorana, clustered	$m = 10 m_{10}$ eV	$m\sigma$	$\sigma = 10^{-3}\sigma_{-3}$

[a] $T = (4/11)^{1/3} \times 2.73$ K.

[b] Solar system speed through cosmic microwave background is $v \approx 370\ \mathrm{km\,s^{-1}} \approx 1.2 \times 10^{-3}$.

TABLE II. Characteristic accelerations, fluctuations, and time scales.

Case	Acceleration[a,b]	Fluctuation[c,d]	Time scale[e,f]
Relativistic	a_u	f_u	t_u
Dirac, unclustered[g] $(mv/T \ll 1)$	$(a_u/v^2)\tilde{m}^2$	$(f_u/v)\tilde{m}$	$t_u v^3/\tilde{m}^3$
Dirac, unclustered $(mv/T \gg 1)$	a_u/v^2	$(f_u/v)\tilde{m}^4$	$t_u v^3 \tilde{m}^4$
Dirac, clustered	a_c	f_c	t_c
Majorana, unclustered $(mv/T \ll 1)$	a_u	$f_u v/\tilde{m}$	$t_u v/\tilde{m}$
Majorana, unclustered $(mv/T \gg 1)$	a_u	$f_u v \tilde{m}^4$	$t_u v \tilde{m}^4$
Majorana, clustered	$a_c\sigma^2$	$f_c\sigma^2$	t_c/σ^2

[a] $a_u = 1.4 \times 10^{-35}\ \mathrm{cm\,s^{-2}}\ (C_V^2 \rho v_{-3}/\mu^2)$, where ρ is in $\mathrm{g\,cm^{-3}}$.
[b] $a_c = 9.2 \times 10^{-24}\ \mathrm{cm\,s^{-2}}\ (C_V^2 \rho \rho_{\nu,0.01} v_{-3}/\mu^2 \sigma_{-3}^2 m_{10})$, where $\rho_\nu = 0.01 M_\odot\ \mathrm{pc^{-3}} \rho_{\nu,0.01}$.
[c] $f_u = (2.8 \times 10^{-28})^2\ \mathrm{cm^2\,s^{-3}}\ (C_V^2/\mu^2)$.
[d] $f_c = (2.5 \times 10^{-20})^2\ \mathrm{cm^2\,s^{-3}}\ (C_V^2 m_{10}^3 \sigma_{-3}^3 \rho_{\nu,0.01}/\mu^2)$.
[e] $t_u = 4.1 \times 10^{14}\ \mathrm{s}\ (\mu^2/C_V^2 \rho^2 v_{-3}^2)$.
[f] $t_c = 7.7 \times 10^6\ \mathrm{s}\ (m_{10}^5 \sigma_{-3}^7 \mu^2/C_V^2 \rho^2 \rho_{\nu,0.01} v_{-3}^2)$.
[g] $\tilde{m} \equiv mv/T = mv_{-3}/0.17\ \mathrm{eV}$.

When fluctuations are more important than mean forces, the already difficult task of uncovering the tiny effects of cosmological neutrinos could be still harder than previously thought.

D. Classical vs quantum

Even though the classical and Born approximation results for $\mathbf{F}$ and dp^2/dt are identical for Dirac neutrinos interacting with large targets, the nature of the interaction is different in the two limits. Classically, the impulses given to the target result from a particle influx at a rate $\sim \pi R^2 n_\nu v_\nu$; each incident neutrino gives the target an impulse determined precisely by its impact parameter $\mathbf{b}$. Because $\mathbf{b}$ is distributed uniformly over the projected area of the target, the distribution of impulses per neutrino with incident momentum $\mathbf{p}_\nu$ has a rms value $\Delta p_{\rm rms} \sim G_F C_V \rho/\mu v_\nu$ and a mean value of magnitude $|\overline{\Delta \mathbf{p}}| \sim (\Delta p_{\rm rms})^2/p_\nu$ oriented along $\mathbf{p}_\nu$. On the other hand, in the Born approximation, the target presents a cross section much smaller than πR^2 to incident neutrinos; the interaction rate is

$$\Gamma_\nu = \frac{G_F^2 C_V^2 M^2}{\mu^2 (2\pi)^5} \int \frac{d^3p_i}{E_i} \frac{d^3p_f}{E_f} N_{\mathbf{p}_i}(1 - N_{\mathbf{p}_f}) W^2 \times (|\mathbf{p}_i - \mathbf{p}_f| R) G_\nu(\mathbf{p}_i, \mathbf{p}_f) \delta(E_f - E_i)\ . \quad (2.45)$$

For a large target, Eq. (2.45) implies $\Gamma_\nu \sim (G_F C_V \rho R/\mu v_\nu)^2 \pi R^2 n_\nu v_\nu$, which is far lower than the classical interaction rate when the Born approximation is valid. However, the rms and mean momentum transfers are correspondingly larger: $\Delta p_{\rm rms} \sim 1/R$ at large R, with $|\overline{\Delta \mathbf{p}}| \sim (\Delta p_{\rm rms})^2/p_\nu$ as before.

The classical interaction rate is approached for either very large targets or exceptionally well-localized incident neutrinos. For Dirac neutrinos, "very large targets" means $G_F C_V \rho R/\mu v_\nu \gtrsim 1$ or $R \gtrsim 4000(\mu v_\nu/C_V \rho)$ km, which is huge by laboratory standards even for clustered neutrinos, with $v_\nu \sim 10^{-3}$ [19]. "Well-localized" neutrinos must have wave functions with a spatial spread $\Delta x \ll R$ and a momentum spread $\Delta p \ll p$ upon entering the target. It is obviously impossible to satisfy both conditions for small targets ($R \lesssim p_\nu^{-1}$). In principle, neutrino localization could play a role for larger targets, but in practice this will not be so. To see why, let us consider the spreading of a wave packet freely propagating from neutrino decoupling. Concentrate on unclustered neutrinos; for clustered neutrinos, the overall spreading will be larger still. The comoving extent $\mathbf{\Delta x}$ of a wave packet with comoving momentum spread $\mathbf{\Delta k}$ about a mean value $\mathbf{k}$ evolves according to

$$\frac{d\mathbf{\Delta x}}{dt} = \frac{k^2 \mathbf{\Delta k}_\perp/a^4 + m^2 \mathbf{\Delta k}/a^2}{(k^2/a^2 + m^2)^{3/2}}\ , \quad (2.46)$$

where $\mathbf{\Delta k}_\perp = \mathbf{\Delta k} - \hat{\mathbf{k}}\hat{\mathbf{k}} \cdot \mathbf{\Delta k}$ and $a(t)$ is the cosmological scale factor, which is defined to be one at the present time. Assuming that $\mathbf{\Delta k}_\perp \neq 0$, most of the growth of $\mathbf{\Delta x}$ occurs while the neutrinos are still relativistic [since the right-hand side (RHS) of Eq. (2.46) is $\sim \mathbf{\Delta k}_\perp/ka$ for $k/a \gg m$ and $\sim \mathbf{\Delta k}/ma^2$ for $k/a \ll m$], and for neutrinos that are nonrelativistic today, we estimate

$$\mathbf{\Delta x} - \mathbf{\Delta x}_d \sim \frac{\mathbf{\Delta k}}{k} \frac{t_m}{a_m}\ , \quad (2.47)$$

where t_m is the age of the Universe when $k/a = m$, $a_m = a(t_m)$, and $\mathbf{\Delta x}_d$ is the spatial extent of the wave packet at neutrino decoupling. [For neutrinos that are still relativistic today, replace $\mathbf{\Delta k}$ by $\mathbf{\Delta k}_\perp$, t_m by t_0, and a_m by 1 in Eq. (2.47).] Since $|\mathbf{\Delta x}_d| \sim |\mathbf{\Delta k}|^{-1}$, Eq. (2.47) implies that the minimum $|\mathbf{\Delta x}|$ is of order

$$\left(\frac{t_m}{ka_m}\right)^{1/2} \sim \left(\frac{t_m}{Ta_m}\right)^{1/2} \sim 10^{12}\Omega_0^{-1/4}h_0^{-1}\ \text{cm} \times \begin{cases} (T/ma_{\rm eq})^{1/4} & \text{if } T/ma_{\rm eq} > 1\ , \\ (T/ma_{\rm eq})^{1/2} & \text{if } T/ma_{\rm eq} < 1\ , \end{cases} \tag{2.48}$$

where Ω_0 is the cosmological closure parameter, h_0 is the Hubble constant in units of 100 $\text{km s}^{-1}\text{Mpc}^{-1}$ and $a_{\rm eq} \approx 4\times10^{-5}(\Omega_0 h_0^2)^{-1}$ is the scale factor when nonrelativistic and relativistic energy densities were equal in standard cosmology; thus, $T/a_{\rm eq} \approx 4\Omega_0 h_0^2$ eV. For neutrinos that are still relativistic today, the minimum spread is orthogonal to $\mathbf{k}$ and of order

$$\left(\frac{t_0}{k}\right)^{1/2} \sim \left(\frac{t_0}{T}\right)^{1/2} \sim 10^{13}h_0^{-1/2}\ \text{cm}\ , \tag{2.49}$$

where $t_0 \sim 10^{10}h_0^{-1}$ yr is the present age of the Universe. These minimum values of $|\Delta\mathbf{x}|$ show that localization of cosmological neutrinos cannot be relevant on the scale of laboratory experiments.

For sufficiently long times t, $\Gamma_\nu t \gg 1$, enough collisions between cosmological neutrinos and the target mass have occurred that the distribution of cumulative impulses given to the probe is approximately Gaussian with a mean $\mathbf{F}t$ and a variance $t\,dp^2/dt$. At times $t > (S/N)^2 t_c$, the Gaussian becomes sharply peaked, with a mean value a factor S/N larger than its width. This general sequence of events is plausible as long as $\Gamma_\nu t_c \gtrsim 1$ (and preferably $\Gamma_\nu t_c \gg 1$ for the central limit theorem to hold rigorously on time scales $\sim t_c$). It is straightforward to evaluate Γ_ν numerically; we rewrite Eq. (2.45) as

$$\Gamma_\nu = \frac{G_F^2 C_V^2 \rho^2 E_\nu n_\nu}{\mu^2 p_\nu^5}\mathcal{R}_D(\hat{R}) \tag{2.50}$$

for Dirac neutrinos and

$$\Gamma_\nu = \frac{G_F^2 C_V^2 \rho^2 n_\nu}{\mu^2 E_\nu p_\nu^3}\mathcal{R}_M(\hat{R}) \tag{2.51}$$

for Majorana neutrinos. In both cases ($\alpha = D$ or M)

$$\Gamma_\nu t_c = \left(\frac{p_\nu}{E_\nu|\mathbf{v}|}\right)^2 \mathcal{R}_\alpha(\hat{R})\mathcal{T}_\alpha(\hat{R})\ ; \tag{2.52}$$

the dot-dashed lines in Figs. 1–7 show $\mathcal{R}_\alpha(\hat{R})\mathcal{T}_\alpha(\hat{R})$ as a function of $\hat{R}$, and Table III lists values at selected $\hat{R}$. At small $\hat{R}$, $\mathcal{R}_\alpha(\hat{R})\mathcal{T}_\alpha(\hat{R}) \approx$ const, whereas at large $\hat{R}$, $\mathcal{R}_\alpha(\hat{R})\mathcal{T}_\alpha(\hat{R}) \approx \hat{R}^2/\ln\hat{R}$ (in the Born approximation). Even for $\hat{R} \approx 1$, $\Gamma_\nu t_c \gtrsim 10$ (except for unclustered neutrinos with $mv/T \gg 1$); $\Gamma_\nu t_c \gg 1$ even for moderately large targets (e.g., $\hat{R} \gtrsim 10$). Typical scattering rates at $\hat{R} \sim 1$ are $\Gamma_\nu \sim (\text{days})^{-1}$ for unclustered Dirac neutrinos with $mv/T \sim 1$, $\Gamma_\nu \sim (\text{days})^{-1}$ for Dirac neutrinos clustered in the galaxy, $\Gamma_\nu \sim (10^4\ \text{yr})^{-1}$ for unclustered Majorana neutrinos with $mv/T \sim 1$, $\Gamma_\nu \sim (10^4\ \text{ys})^{-1}$ for Majorana neutrinos clustered in the galaxy, and $\Gamma_\nu \sim (10\ \text{yr})^{-1}$ for extremely relativistic neutrinos. Obviously, these time scales are too long for practical detection schemes except for clustered Dirac neutrinos or unclustered Dirac neutrinos with $mv/T \sim 1$. For target scattering rates of order one per day, detectors with $\hat{R} \sim 1$ may be used for either clustered Dirac neutrinos or unclustered Dirac neutrinos with $mv/T \sim 1$, detectors with $\hat{R} \sim 50$ must be used for either clustered Majorana neutrinos [$R \approx 0.02\hat{R}/m(\text{eV})\sigma_{-3}$ cm] or unclustered Majorana neutrinos with $mv/T \sim 1$ ($R \approx 0.12\hat{R}T/mv$ cm), and detectors with $\hat{R} \sim 10$ must be used for extremely relativistic neutrinos ($R \approx 0.12\hat{R}$ cm).

E. Other geometries

Throughout this section, we have assumed that the laboratory target mass is spherical. We have done so mainly as a matter of convenience: The resulting expressions for $\mathbf{F}$, dp^2/dt, and Γ_ν depend on the size of the detector only through a single parameter, $\hat{R} = \bar{\rho}R$. It is easy to recover Born approximations to these quantities for detectors of arbitrary shape by replacing the vector form factor for a sphere, $W_V(|\mathbf{p}_i - \mathbf{p}_f|)$, introduced in Eqs. (2.28) and (2.29) by the more general

$$W_V(\mathbf{p}_i - \mathbf{p}_f) = C_V \int_{\mathcal{V}} d^3r \frac{\rho}{M} e^{i(\mathbf{p}_i - \mathbf{p}_f)\cdot\mathbf{r}}\ , \tag{2.53}$$

where the integral is over the target volume $\mathcal{V}$; indeed, it is also easy to include nonuniform target density profiles in Eq. (2.53). For example, if the scatterer is a uniformly dense rectangular solid whose sides have lengths L_1, L_2, and L_3, then it is easy to see that

$$W_V(\mathbf{p}_i - \mathbf{p}_f) = C_V \prod_{\alpha=1,2,3} \frac{\sin[(p_{i,\alpha} - p_{f,\alpha})L_\alpha/2]}{(p_{i,\alpha} - p_{f,\alpha})L_\alpha/2}\ . \tag{2.54}$$

Obviously, the evaluation of steady and nonsteady forces is more complicated in rectangular geometry than in spherical geometry, since the extent of the source in each of three dimensions may differ from the other two, and

TABLE III. Selected values of $\mathcal{R}_D(\hat{R})\mathcal{T}_D(\hat{R})$ and $\mathcal{R}_M(\hat{R})\mathcal{T}_M(\hat{R})$.

Case	$\hat{R} = 0.01$	$\hat{R} = 1.0$	$\hat{R} = 100$
Relativistic	0.866	10.0	2.94×10^4
Dirac, unclustered ($mv/T \ll 1$)	22.0	55.7	7.26×10^4
Dirac, unclustered ($mv/T \gg 1$)	2.00	2.33	3.59×10^3
Dirac, clustered	8.73	23.9	5.42×10^4
Majorana, unclustered ($mv/T \ll 1$)	31.3	1.43×10^2	3.33×10^5
Majorana, unclustered ($mv/T \gg 1$)	3.00	3.45	3.95×10^3
Majorana, clustered	11.2	32.5	7.63×10^4

the final results will depend, in general, on L_1, L_2, and L_3 separately. For comparable dimensions $L_1 \sim L_2 \sim L_3$, we expect our spherical results to be adequate within geometrical factors ~ 1. We can recover the oft-studied [6–8,10,11] "slab geometry" by assuming that two of the lengths, say, L_1 and L_2, far exceed the third, say, L_3, and are also much larger than typical values of the neutrino momentum in the 1,2 plane [20]. In this limit, it is easily shown that $\mathbf{F}$, dp^2/dt, and Γ_ν are all proportional to the slab area, $A = L_1 L_2$. Thus the characteristic time scale for the signal due to $\mathbf{F}$ to exceed the noise due to dp^2/dt is proportional to $1/A$ and may be small. Note that this behavior is not unlike the $(\hat{R}^2 \ln \hat{R})^{-1}$ scaling obeyed by t_c for spheres with large $\hat{R}$.

For clustered Dirac neutrinos, we find

$$\mathbf{a} \approx \hat{\mathbf{e}}_3 \frac{G_F^2 C_V^2 \rho \rho_\nu}{\mu^2 \sigma} \mathcal{F}_D^{(s)}(\hat{L}_3, v_3/\sigma) \tag{2.55}$$

and

$$\frac{dv^2}{dt} \approx \frac{2 G_F^2 C_V^2 \rho_\nu m \sigma}{\mu^2 A} \mathcal{G}_D^{(s)}(\hat{L}_3, v_3/\sigma) \ , \tag{2.56}$$

where $\hat{L}_3 \equiv m\sigma L_3$, $v_3 = \hat{\mathbf{e}}_3 \cdot \mathbf{v}$ is the component of the mean neutrino velocity $\mathbf{v}$ along $\hat{\mathbf{e}}_3$,

$$\mathcal{F}_D^{(s)}(L, v) = L^{-1} \int_{-\infty}^{+\infty} \frac{dx}{\sqrt{2\pi}} \frac{x \sin^2(xL)}{|x|^3} \exp[-\tfrac{1}{2}(x - v)^2] \tag{2.57}$$

and

$$\mathcal{G}_D^{(s)}(L, v) = L^{-2} \int_{-\infty}^{+\infty} \frac{dx}{\sqrt{2\pi}} \frac{\sin^2(xL)}{|x|} \exp[-\tfrac{1}{2}(x - v)^2] \ . \tag{2.58}$$

Figure 8 shows the results of numerical evaluation of Eqs. (2.55) and (2.56) for $v_3 = \sqrt{2}\sigma$. Note that at small values of $\hat{L}_3$, $\mathcal{F}_D^{(s)}(\hat{L}_3, v_3/\sigma) \sim \hat{L}_3$, and $\mathcal{G}_D^{(s)}(\hat{L}_3, v_3/\sigma) \sim$ const and that at large values of $\hat{L}_3$, $\mathcal{F}_D^{(s)}(\hat{L}_3, v_3/\sigma) \sim \hat{L}_3^{-1} \ln \hat{L}_3$, and $\mathcal{G}_D^{(s)}(\hat{L}_3, v_3/\sigma) \sim \hat{L}_3^{-2} \ln \hat{L}_3$.

III. CORRELATED MOTIONS OF A PAIR OF TARGET MASSES

A. Two-point correction function for accelerations

Let us consider a simplified model for the interaction of either extremely relativistic or nonrelativistic Dirac neutrinos with a pair of targets $i = 1, 2$. If $\hat{\phi}_i(\mathbf{x}, t)$ is the field operator that destroys target i centered at position $\mathbf{x}$, and $\hat{\psi}_\nu(\mathbf{x}, t)$ is the analogous neutrino operator, the Hamiltonian is

$$H = H_{\text{free}} + \sum_{i=1}^{2} \int d^3x \, d^3x' \, \hat{\phi}_i^\dagger(\mathbf{x}, t) \hat{\phi}_i(\mathbf{x}, t) U_i(\mathbf{x} - \mathbf{x}') \hat{\psi}_\nu^\dagger(\mathbf{x}', t) \hat{\psi}(\mathbf{x}', t) \ , \tag{3.1}$$

where H_{free} is the Hamiltonian for the free fields and $U_i(\mathbf{x} - \mathbf{x}')$ is only nonzero inside the volume occupied by target i. It is straightforward to find the time evolution equations for $\hat{\phi}_i(\mathbf{x})$ and $\hat{\psi}_\nu(\mathbf{x})$ from Eq. (3.1), and it follows that the force experienced by target i is the expectation value of the operator

$$\hat{\mathbf{F}}_i = -\int d^3x \, \hat{\phi}_i^\dagger(\mathbf{x}, \mathbf{t}) \hat{\phi}_i(\mathbf{x}, t) \frac{\partial}{\partial \mathbf{x}} \int d^3x' U_i(\mathbf{x} - \mathbf{x}') \hat{\psi}_\nu^\dagger(\mathbf{x}', t) \hat{\psi}_\nu(\mathbf{x}', t) \ . \tag{3.2}$$

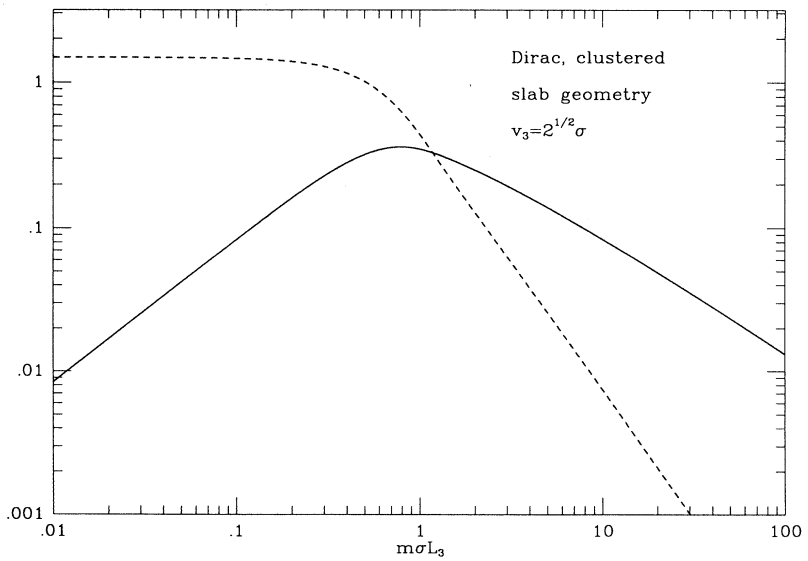

FIG. 8. Dimensionless acceleration $\mathcal{F}_D^{(s)}(\hat{L}_3, v/\sigma)$ (solid line) and fluctuation $\mathcal{G}_D^{(s)}(\hat{L}_3, v/\sigma)$ (dashed line) for slab geometry, assuming $v/\sigma = \sqrt{2}$.

From Eq. (3.2) we deduce that $\mathbf{F}_i = \langle \hat{\mathbf{F}}_i \rangle = 0$ for a uniform gas of neutrinos to first order in the interaction potential, as we have seen in Sec. II, just as was shown by Cabibbo and Maiani [6] for a similar interaction Hamiltonian and in a time-average sense by Langacker, Leveille, and Sheiman [5]. The lowest-order nonzero $\mathbf{F}_i$ is due to perturbations of the neutrino wave functions by the targets themselves. It is sufficient to employ unperturbed states for the targets, which we henceforth take to be well localized at positions $\mathbf{x}_i$.

The steady accelerations of target masses by background neutrinos are extremely small; moreover, fluctuating accelerations could dominate on reasonable laboratory time scales. For a single-target mass, the fluctuations constitute an irreducible source of noise, present even if all other sources of random impulses have been eliminated. We expect, though, that the fluctuating accelerations of a pair of nearby masses should be correlated with one another, with a correlation length scale $\sim p_\nu^{-1}$. (The steady accelerations, which point in the same direction, are obviously correlated.) These correlations could facilitate detection of the fluctuating accelerations.

The two-point correlation function for the force is the expectation value of the operator

$$\hat{F}_{12}^2 = \frac{\partial^2}{\partial x_1^i \partial x_2^i} \int d^3x_1' \, d^3x_2' \langle \hat{C}(\mathbf{x}_1 + \mathbf{x}_1', t_1; \mathbf{x}_2 + \mathbf{x}_2', t_2) \rangle \ , \tag{3.3}$$

where $\langle \hat{\mathcal{O}} \rangle$ (for any operator $\mathcal{O}$) is computed in the neutrino background; the density fluctuation $\langle \hat{C}(x_1, x_2) \rangle$ is computed in the Appendix. Introducing Fourier transforms, we find, for a pair of inequivalent spherical targets,

$$\frac{\langle \hat{F}_{12}^2 \rangle}{M_1 M_2} = \frac{\xi^2 G_F^2 C_{V,1} C_{V,2}}{\mu_1 \mu_2} \int d^3q \, d^3\sigma \, q^2 W(qR_1) W(qR_2) [e^{i(\mathbf{q}\cdot\mathbf{x} - \sigma t)} n_a^2(\mathbf{q}, \sigma) + e^{-i(\mathbf{q}\cdot\mathbf{x} - \sigma t)} n_a^2(-\mathbf{q}, -\sigma)] \ , \tag{3.4}$$

where $\mathbf{x} \equiv \mathbf{x}_1 - \mathbf{x}_2$ and $t = t_1 - t_2$; $n_a^2(\mathbf{q}, \sigma)$ is given by Eq. (A6), and $\xi = \sqrt{2}$ for extremely relativistic neutrinos and $\xi = 1/\sqrt{2}$ for nonrelativistic Dirac neutrinos. If t is large compared to the correlation time scale for density fluctuations in the neutrino background, we can replace $n_a^2(\pm\mathbf{q}, \pm\sigma)$ with $n_a^2(\pm\mathbf{q}, 0)$ in the integral; we then find that the correlation function for a pair of targets is approximately

$$\frac{\langle \tilde{F}_{12}^2 \rangle}{M_1 M_2} = \delta(t_1 - t_2) a_{12}(\mathbf{x}_1 - \mathbf{x}_2) \ , \tag{3.5}$$

where

$$a_{12}(\mathbf{x}) = \frac{\pi \xi^2 G_F^2 C_{V,1} C_{V,2}}{\mu_1 \mu_2} \int d^3q \, q^2 W(qR_1) W(qR_2) [e^{i\mathbf{q}\cdot\mathbf{x}} n_a^2(\mathbf{q}, 0) + e^{-i\mathbf{q}\cdot\mathbf{x}} n_a^2(\mathbf{q}, 0)] \ . \tag{3.6}$$

A semiclassical, heuristic argument may also be used to derive Eq. (3.6) and suggests its generalization to Majorana neutrinos. Let

$$\delta\mathbf{F}(\mathbf{x}_i, t) = C_{V,i} \int d^3x \frac{\rho(\mathbf{x})}{\mu_i} \mathbf{f}(\mathbf{x}_i + \mathbf{x}, t) \tag{3.7}$$

be the fluctuating force on mass i centered at position $\mathbf{x}_i$. Introduce the Fourier decomposition

$$\mathbf{f}(\mathbf{x}, t) = \int d^3q \, \tilde{\mathbf{f}}(\mathbf{q}, t) e^{i\mathbf{q}\cdot\mathbf{x}} \tag{3.8}$$

into Eq. (3.8); the fluctuating acceleration of the target is then

$$\delta\mathbf{a}(\mathbf{x}_i, t) = \frac{1}{\mu_i} \int d^3q \, e^{i\mathbf{q}\cdot\mathbf{x}_i} \tilde{\mathbf{f}}(\mathbf{q}, t) W_{V,i}(\mathbf{q}) \ , \tag{3.9}$$

where $W_{V,i}(\mathbf{q})$ is the vector form factor for target i. For time scales long compared to the correlation time of density fluctuations in the neutrino background, we may approximate

$$\langle \tilde{\mathbf{f}}(\mathbf{q}', t') \cdot \tilde{\mathbf{f}}(\mathbf{q}, t) \rangle = \delta^{(3)}(\mathbf{q} + \mathbf{q}') \delta(t - t') \tilde{f}^2(\mathbf{q}) \ , \tag{3.10}$$

and so the correlation function for the fluctuating accelerations of a pair of masses (1,2) is

$$\langle \delta\mathbf{a}(\mathbf{x}_1, t_1) \cdot \delta\mathbf{a}(\mathbf{x}_2, t_2) \rangle = \delta(t_1 - t_2) a_{12}(\mathbf{x}_1 - \mathbf{x}_2) \ , \tag{3.11}$$

where

$$a_{12}(\mathbf{r}) = \frac{1}{\mu_1 \mu_2} \int d^3q \, e^{i\mathbf{q}\cdot\mathbf{r}} \tilde{f}^2(\mathbf{q}) W_{V,1}(\mathbf{q}) W_{V,2}^*(\mathbf{q}) \ . \tag{3.12}$$

When 1 and 2 are actually the same target mass [i.e., $W_{V,1}(\mathbf{q}) = W_{V,2}(\mathbf{q}) = W_V(\mathbf{q})$ and $\mathbf{r} = 0$], $a_{12}^2(\mathbf{r})$ must reduce to dv^2/dt; moreover, since $a_{12}(\mathbf{r})$ and $\tilde{f}^2(\mathbf{q})$ are both real, $\tilde{f}^2(-\mathbf{q}) = \tilde{f}^2(\mathbf{q})$. With the aid of Eq. (2.29), we deduce that

$$\tilde{f}^2(\mathbf{q}) = \frac{G_F^2 q^2}{2(2\pi)^5} \int \frac{d^3p_i}{E_i} \frac{d^3p_f}{E_f} N_{\mathbf{p}_i} (1 - N_{\mathbf{p}_f}) G_\nu(\mathbf{p}_i, \mathbf{p}_f) \delta(E_f - E_i) [\delta^{(3)}(\mathbf{p}_i - \mathbf{p}_f - \mathbf{q}) + \delta^{(3)}(\mathbf{p}_i - \mathbf{p}_f + \mathbf{q})] \tag{3.13}$$

satisfies both requirements. For either relativistic neutrinos or nonrelativistic Dirac neutrinos, Eq. (3.13) is identical to Eq. (3.6).

In Fig. 9, we show numerical results for $a_{12}(\mathbf{r})$ for extremely relativistic neutrinos interacting with a pair of spherical masses of different composition but identical radii R. The correlation function is evaluated to zeroth order in $v \sim 10^{-3}$; corrections are $O(v^2)$. This specific case illustrates two general features of $a_{12}(\mathbf{r})$: (1) Correlations are largest for small spheres ($\hat{R} \ll 1$) separated by small distances ($2\hat{R} \leq \hat{r} \ll 1$); (2) at $\hat{r} \gg 1$, $|a_{12}(\mathbf{r})| \sim \hat{r}^{-4}$. [In fact, $a_{12}(\mathbf{r}) < 0$ for extremely relativistic neutrinos at large $\hat{r}$; if the resolution were better in the figure, the cusps evident for $\hat{R} = \frac{1}{8}$ and $\frac{1}{4}$ would in fact be seen to be zero crossings.] For nonrelativistic neutrinos with $mv \gtrsim \bar{p}$, $a_{12}(\mathbf{r})$ will depend in general on the angle between $\mathbf{v}$ and $\mathbf{r}$. Majorana neutrinos interacting with polarized targets whose net electron spins are $\langle \mathbf{s}_{e,i} \rangle$ should have $a_{12}(\mathbf{r}) \propto \langle \mathbf{s}_{e,1} \rangle \cdot \langle \mathbf{s}_{e,2} \rangle$.

B. "Shadowing force" due to scattered waves

A particular consequence of Eq. (3.2) is that the first-order forces $\mathbf{F}_i$ are identically zero for an incident plane wave. The second-order forces are nonzero because, loosely speaking, the scattered waves that result from the interaction of the incident neutrino with the targets result in small gradients in the neutrino density. The interaction of target i with its own scattered wave is responsible for the $O(G_F^2)$ forces evaluated in Sec. II. The interaction of target i with the wave scattered by $j \neq i$ leads to a kind of second-order "shadowing force," that is, a relative acceleration polarized with respect to the vector separation of the targets, $\mathbf{r} = \mathbf{r}_1 - \mathbf{r}_2$. This force may be either attractive or repulsive, as we shall see.

For the purpose of computing the perturbation of an incident neutrino by the localized targets, it suffices to replace the targets with static potentials and to use stationary perturbation theory. Doing so, we find that the force felt by target 1 due to the scattered wave from target 2 is

$$\mathbf{F}_{12} = -\frac{\partial}{\partial \mathbf{r}_1} V(\mathbf{r}_1 - \mathbf{r}_2) \ , \tag{3.14}$$

where, for targets bathed in a neutrino phase space distribution $N_{\mathbf{k}}$,

$$V(\mathbf{r}) = -\frac{1}{\pi} \int d^3x_1 d^3x_2 U_1(\mathbf{x}_1) U_2(\mathbf{x}_2) \Psi(\mathbf{r} + \mathbf{x}_1 - \mathbf{x}_2) \tag{3.15}$$

and ($E_k = \sqrt{k^2 + m^2}$)

$$\Psi(\mathbf{R}) = \frac{1}{R} \int \frac{d^3k}{(2\pi)^3} N_{\mathbf{k}} E_k \cos(\mathbf{k} \cdot \mathbf{R} - kR) \ . \tag{3.16}$$

For isotropic $N_{\mathbf{k}}$, $V(\mathbf{r}) = V(r)$ and the force is central, but for anisotropic $N_{\mathbf{k}}$ the force depends on the angle between $\mathbf{r}$ and the mean neutrino momentum; in all cases, $\mathbf{F}_{21} = -\mathbf{F}_{12}$.

For any $N_{\mathbf{k}}$, isotropic or not,

$$\Psi(\mathbf{R}) = \frac{\rho_\nu}{R} \tag{3.17}$$

for $p_\nu R \ll 1$, where ρ_ν is the neutrino energy density. For a pair of small spherical targets, we find that, at small separations,

$$V(\mathbf{r}) \approx -\frac{\xi^2 G_F^2 C_{V,1} C_{V,2} M_1 M_2 \rho_\nu}{\pi \mu_1 \mu_2 r} \ , \tag{3.18}$$

where M_i and μ_i are the total mass and mass per atom of target i. Shadowing forces are weaker than the gravitational forces between the targets by the dimensionless factor

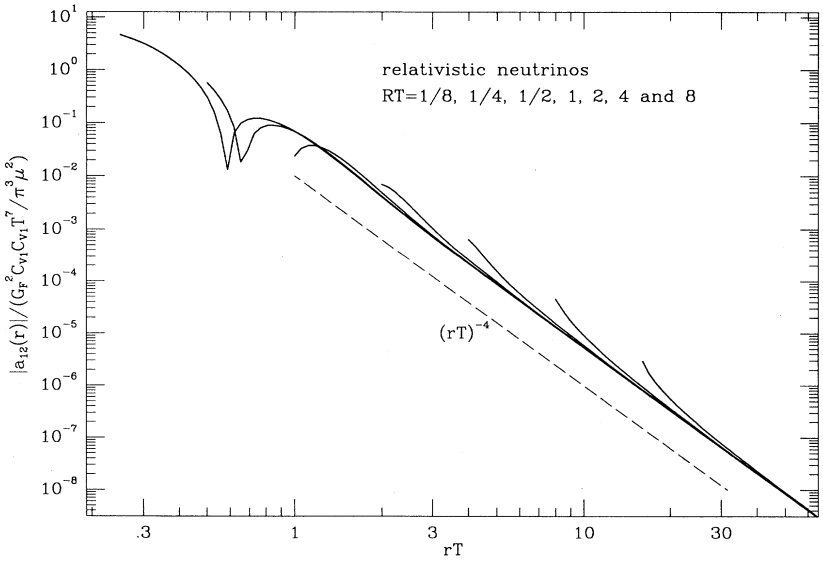

FIG. 9. Two-point correlation function for fluctuating accelerations $a_{12}(r)$ due to extremely relativistic neutrinos calculated to lowest (zeroth) order in the peculiar velocity $\mathbf{v}$. The various solid curves are for pairs of spherical targets of identical radius $RT = \frac{1}{8}, \frac{1}{4}, \frac{1}{2}, 1, 2, 4, 8$. The dashed line shows the asymptotic scaling $a_{12}(r) \propto (rT)^{-4}$ valid at large values of rT.

$$\frac{\xi^2 G_F^2 C_{V,1} C_{V,2} \rho_\nu}{\pi \mu_1 \mu_2} \approx \begin{cases} 3.5 \times 10^{-24} C_{V,1} C_{V,2}/\mu_1\mu_2 \ \text{(extremely relativistic)} , \\ 1.7 \times 10^{-14} C_{V,1} C_{V,2} \rho_{\nu,0.01}/\mu_1\mu_2 \ \text{(nonrelativistic, Dirac)} , \end{cases} \tag{3.19}$$

where μ_i are in units of the proton mass and $\rho_\nu = 0.01 \rho_{\nu,0.01} M_\odot \ \mathrm{pc}^{-3}$. Nevertheless, shadowing forces for small targets within a distance $r \sim p_\nu^{-1}$ of one another may be comparable to or perhaps larger than the forces on individual, more widely separated targets: from Eqs. (3.14) and (3.18), we find accelerations on such scales of order

$$a_1 \approx \frac{3\xi^2 G_F^2 C_{V,1} C_{V,2} \rho_2 \rho_\nu}{4\pi^2 \mu_1 \mu_2 p_\nu} . \tag{3.20}$$

For clustered Dirac neutrinos, Eq. (3.20) is comparable to the peak value of Eq. (2.36), but for extremely relativistic neutrinos, Eq. (3.20) exceeds the peak value of Eq. (2.36) by a factor $\sim |\mathbf{v}|^{-1} \sim 10^3$.

On larger scales, $V(\mathbf{r})$ diminishes rapidly with distance and may even become repulsive. To see how this comes about, focus on isotropic phase space distributions, for which

$$\Psi(\mathbf{R}) = \frac{1}{4\pi^2 R^2} \int_0^\infty dk\, k N_k E_k \sin(2kR) . \tag{3.21}$$

The integral may be done analytically for two interesting cases: (1) extremely relativistic neutrinos, for which $N_k = (e^{k/T} + 1)^{-1}$, and (2) nonrelativistic Dirac neutrinos with $N_k = N_0 e^{-k^2/2p_0^2}$. For extremely relativistic neutrinos, we find

$$\Psi(\mathbf{R}) = \frac{T^3}{4\pi^2 R^2} \mathcal{H}_{\mathrm{ER}}(2\hat{R}) , \tag{3.22}$$

where $\hat{R} = TR$ and

$$\mathcal{H}_{\mathrm{ER}} = -\frac{1}{y^3} + \frac{\pi^3}{\sinh^3(\pi y)} + \frac{\pi^3}{2\sinh(\pi y)} \approx \begin{cases} 7\pi^4 y/120 \ (y \ll 1) , \\ -1/y^3 \ \ (y \gg 1) ; \end{cases} \tag{3.23}$$

clearly, $V(r)$ is repulsive at large r and proportional to r^{-5}. For nonrelativistic Dirac neutrinos, we find

$$\Psi(\mathbf{R}) = \frac{N_0 m p_0^2}{4\pi^2 R^2} \mathcal{H}_{\mathrm{NR}}(2\hat{R}) , \tag{3.24}$$

where now $\hat{R} = p_0 R$ and

$$\mathcal{H}_{\mathrm{NR}}(y) = \sqrt{\pi/2}\, y e^{-y^2/2} ; \tag{3.25}$$

in this case, the potential is always attractive, but decreases extremely rapidly at large r.

Equations (3.15) and (3.16) can also be used to evaluate the shadowing force for nonspherical masses. For example, consider the acceleration of a small object relative to a large, thin slab; let the object be at position $z\hat{\mathbf{e}}_z$ relative to the center of the slab. If the thicknesses of both the slab and small object are small compared to z, then the shadowing force on M is

$$\mathbf{F} = -\hat{\mathbf{e}}_z \frac{\xi^2 G_F^2 C_{V,1} C_{V,2} y_1 M_2}{2\pi^2 \mu_1 \mu_2} \int_0^\infty dk\, k E_k N_k \frac{\sin(2kz)}{z} \tag{3.26}$$

for an isotropic neutrino gas; in Eq. (3.26), we have labeled the slab 1 and the mass 2, and y_1 is the column density of the slab (i.e., for a uniform slab of density ρ_1 and thickness $L_1, y_1 = \rho_1 L_1$). When $\bar{p}z \ll 1$, Eq. (3.26) implies a force

$$\mathbf{F} \approx -\hat{\mathbf{e}}_z \frac{2\xi^2 G_F^2 C_{V,1} C_{V,2} y_1 M_2 \rho_\nu}{\mu_1 \mu_2} . \tag{3.27}$$

For extremely relativistic neutrinos, Eq. (3.26) implies

$$\mathbf{F} = -\hat{\mathbf{e}}_z \frac{G_F^2 C_{V,1} C_{V,2} y_1 M_2 T^3}{\pi^2 \mu_1 \mu_2} \frac{\mathcal{H}_{\mathrm{ER}}(2Tz)}{z} , \tag{3.28}$$

where $\mathcal{H}_{\mathrm{ER}}(y)$ is given by Eq. (3.25), and for nonrelativistic Dirac neutrinos with $N_k = N_0 e^{-k^2/2p_0^2}$, Eq. (3.26) implies

$$\mathbf{F} = -\hat{\mathbf{e}}_z \frac{G_F^2 C_{V,1} C_{V,2} y_1 M_2 \rho_\nu}{\mu_1 \mu_2} e^{-2p_0^2 z^2} . \tag{3.29}$$

Once again, we see that the shadowing force may be either attractive or repulsive (although it is always attractive for nonrelativistic Dirac neutrinos), is very weak compared to gravity [with a relative strength given by Eq. (3.19) at separations $\ll 1/\bar{p}$], and is short range (with a characteristic length scale $\sim 1/\bar{p}$).

IV. EXCITATIONS OF INTERNAL MODES OF A SOLID

A complex system such as a solid will possess internal modes which may be excited by cosmological neutrinos. Generically, we expect only acoustic modes to be excited in a solid or metal, since the characteristic frequencies of either optical or plasma modes is much higher ($\sim$ eV) than the characteristic neutrino energies [21]. In this section, we focus on the interaction of either extremely relativistic or nonrelativistic Dirac neutrinos with a discrete atomic lattice containing N atoms whose unperturbed positions are $\mathbf{x}_j^{(0)}$. Let the interaction Hamiltonian be

$$H' = -\xi G_F C_V \sum_j \delta^{(3)}(\mathbf{x} - \mathbf{x}_j) . \tag{4.1}$$

For this interaction Hamiltonian, the rate of single phonon excitations of a particular normal mode of the lattice from the ground state is

$$R^{(0)}_{\mathbf{k}\lambda} = \frac{\pi\xi^2 G_F^2 C_V^2}{\mu\omega_{\mathbf{k}\lambda}} \int \frac{d^3p}{(2\pi)^3}\frac{d^3p'}{(2\pi)^3} N_{\mathbf{p}}(1-N_{\mathbf{p}'})\delta(E_{\mathbf{p}'}+\omega_{\mathbf{k}\lambda}-E_{\mathbf{p}}) \left|\sum_j \langle 1,\mathbf{k}\lambda|e^{i(\mathbf{p}-\mathbf{p}')\cdot(\mathbf{x}_j^{(0)}+\mathbf{u}_j)}|0\rangle\right|^2 , \tag{4.2}$$

where we have substituted $\mathbf{x}_j = \mathbf{x}_j^{(0)} + \mathbf{u}_j$. For small displacements, we can expand each exponential in the sum to get ($\mathbf{q} \equiv \mathbf{p} - \mathbf{p}'$)

$$i\mathbf{q}\cdot\sum_j e^{i\mathbf{q}\cdot\mathbf{x}_j^{(0)}}\langle 1,\mathbf{k}\lambda|\mathbf{u}_j|0\rangle , \tag{4.3}$$

where the displacement operator is [22]

$$\mathbf{u}_j = \sum_{\mathbf{k}\lambda}(2\mu\omega_{\mathbf{k}\lambda})^{-1/2}[\mathbf{u}_{\mathbf{k}\lambda}(\mathbf{x}_j^{(0)})a_{\mathbf{k}\lambda} + \mathbf{u}^*_{\mathbf{k}\lambda}(\mathbf{x}_j^{(0)})a^\dagger_{\mathbf{k}\lambda}] ; \tag{4.4}$$

in Eq. (4.4), $a_{\mathbf{k}\lambda}$ and $a^\dagger_{\mathbf{k}\lambda}$ are the annihilation and creation operators for mode $\mathbf{k}\lambda$ and $\mathbf{u}_{\mathbf{k}\lambda}(\mathbf{x}_j^{(0)})$ are the classical displacement eigenvectors, which satisfy the orthonormality condition

$$\sum_j \mathbf{u}^*_{\mathbf{k}'\lambda'}(\mathbf{x}_j^{(0)})\cdot\mathbf{u}_{\mathbf{k}\lambda}(\mathbf{x}_j^{(0)}) = \delta_{\mathbf{k},\mathbf{k}'}\delta_{\lambda,\lambda'} . \tag{4.5}$$

Computing the matrix elements, we find that

$$R^{(0)}_{\mathbf{k}\lambda} = \frac{\pi\xi^2 G_F^2 C_V^2 \rho}{\mu^2\omega_{\mathbf{k}\lambda}} \int \frac{d^3p}{(2\pi)^3}\frac{d^3p'}{(2\pi)^3} N_{\mathbf{p}}(1-N_{\mathbf{p}'})|(\mathbf{p}-\mathbf{p}')\cdot\mathbf{V}^d_{\mathbf{k}\lambda}(\mathbf{p}-\mathbf{p}')|^2\delta(E_{\mathbf{p}'}+\omega_{\mathbf{k}\lambda}-E_{\mathbf{p}}) , \tag{4.6}$$

where

$$\mathbf{V}^d_{\mathbf{k}\lambda}(\mathbf{q}) \equiv \sqrt{\mu/\rho}\sum_j e^{i\mathbf{q}\cdot\mathbf{x}_j^{(0)}}\mathbf{u}_{\mathbf{k}\lambda}(\mathbf{x}_j^{(0)}) . \tag{4.7}$$

Since $|\mathbf{q}|\times$(interparticle spacing) $\ll 1$ for all likely momentum transfers $\mathbf{q}$, we can turn the sums over j into volume integrals by replacing $\sum_j \to (\rho/\mu)\int d^3x$; in doing so, we can define continuous eigenvectors

$$\mathbf{u}^{(c)}_{\mathbf{k}\lambda} \equiv (\rho/\mu)^{1/2}\mathbf{u}_{\mathbf{k}\lambda}(\mathbf{x}) , \tag{4.8}$$

which obey the normalization condition

$$\int d^3x\, \mathbf{u}^*_{\mathbf{k}'\lambda'}(\mathbf{x})\cdot\mathbf{u}_{\mathbf{k}\lambda}(\mathbf{x}) = \delta_{\mathbf{k},\mathbf{k}'}\delta_{\lambda,\lambda'} . \tag{4.9}$$

In the continuum limit, the excitation rate becomes

$$R^{(0)}_{\mathbf{k}\lambda} = \frac{\pi\xi^2 G_F^2 C_V^2 \rho}{\mu^2\omega_{\mathbf{k}\lambda}} \int \frac{d^3p}{(2\pi)^3}\frac{d^3p'}{(2\pi)^3} N_{\mathbf{p}}(1-N_{\mathbf{p}'})|(\mathbf{p}-\mathbf{p}')\cdot\mathbf{V}^{(c)}_{\mathbf{k}\lambda}(\mathbf{p}-\mathbf{p}')|^2\delta(E_{\mathbf{p}}-E_{\mathbf{p}'}-\omega_{\mathbf{k}\lambda}) , \tag{4.10}$$

where

$$\mathbf{V}^{(c)}_{\mathbf{k}\lambda}(\mathbf{q}) \equiv \int d^3x\, e^{i\mathbf{q}\cdot\mathbf{x}}\mathbf{u}^{(c)}_{\mathbf{k}\lambda}(\mathbf{x}) ; \tag{4.11}$$

henceforth, we drop the superscript c.

Exact values of $R^{(0)}_{\mathbf{k}\lambda}$ will depend on the spectrum of normal modes and therefore on the symmetries of the solid (which determine the number of independent elastic moduli) [23]. On intuitive grounds, we expect that the largest response at a given wave vector $\mathbf{k}$ will be for longitudinally polarized normal modes, since the driving force is the gradient of a potential. In a real crystal, of course, none of the three modes at a given $\mathbf{k}$ is precisely longitudinal or precisely transverse, but usually one of the modes is nearly longitudinal. To keep the evaluation of $R^{(0)}_{\mathbf{k}\lambda}$ as simple as possible, we shall idealize to an isotropic medium, in which one of the modes is precisely longitudinal (with a dispersion relation $\omega^2_{\mathbf{k}l} = k^2c_l^2$) and the other two are precisely transverse (and degenerate, with $\omega^2_{\mathbf{k}t} = k^2c_t^2$). For an isotropic medium, $\mathbf{u}_{\mathbf{k}l} = k^{-2}\nabla\delta_{\mathbf{k}l}$, where $\delta_{\mathbf{k}l}(\mathbf{x})$ is the density contrast in the longitudinal mode. We consider two different possible boundary conditions on the density: "free" boundary conditions, for which $\delta_{\mathbf{k}l}(\mathbf{x}) = 0$ on the surface, and "fixed" boundary conditions, for which $\hat{\mathbf{n}}\cdot\nabla\delta_{\mathbf{k}l}(\mathbf{x})0$ on the surface. More complicated choices are possible (some surfaces fixed, others free), but we expect that considering these two alternatives should suffice for determining whether or not

the excitation rates depend sensitively on boundary conditions.

To be precise, let us assume that the solid is a rectangular solid with side lengths L_x, L_y, L_z which need not be the same. Let the solid extend over $x = [0, L_x]$, $y = [0, L_y]$, and $z = [0, L_z]$; we may take

$$\frac{1}{k}\delta_{\mathbf{k}\lambda}(\mathbf{x}) = \begin{cases} \sqrt{8/V}\cos(k_x x)\cos(k_y y)\cos(k_z z) & \text{(fixed)}\ , \\ \sqrt{8/V}\sin(k_x x)\sin(k_y y)\sin(k_z z) & \text{(free)}\ , \end{cases}$$

where V is the volume of the solid and in both cases $k_x = n_x\pi/L_x$, $k_y = n_y\pi/L_y$, and $k_z = n_z\pi/L_z$ with n_x, n_y, and n_z positive integers. It is then straightforward to show that

$$|i\mathbf{q}\cdot\mathbf{V}_{\mathbf{k}l}(\mathbf{q})|^2 = k^2 \prod_{i=x,y,z}\frac{L_i}{2}\left\{\frac{4q_i\sin[\frac{1}{2}(q_i-k_i)L_i]}{(q_i^2-k_i^2)L_i}\right\}^2 \tag{4.12}$$

for fixed ends and

$$|i\mathbf{q}\cdot\mathbf{V}_{\mathbf{k}l}(\mathbf{q})|^2 = \frac{q^4}{k^2}\prod_{i=x,y,z}\frac{L_i}{2}\left\{\frac{4k_i\sin[\frac{1}{2}(q_i-k_i)L_i]}{(q_i^2-k_i^2)L_i}\right\}^2 \tag{4.13}$$

for free ends. In each case, the quantity in brackets is extremely sharply peaked at $q_i = \pm k_i$, where it approaches one; if we neglect the tails of these functions, we may approximate

$$|i\mathbf{q}\cdot\mathbf{V}_{\mathbf{k}l}(\mathbf{q})|^2 = \pi^3 k^2 \prod_{i=x,y,z}[\delta(q_i-k_i)+\delta(q_i+k_i)] \tag{4.14}$$

for fixed ends and

$$|i\mathbf{q}\cdot\mathbf{V}_{\mathbf{k}l}(\mathbf{q})|^2 = \pi^3\frac{q^4}{k^2}\prod_{i=x,y,z}[\delta(q_i-k_i)+\delta(q_i+k_i)] \tag{4.15}$$

for free ends. Note that for large q, if all components of q are comparable, $|i\mathbf{q}\cdot\mathbf{V}_{\mathbf{k}l}(\mathbf{q})|^2 \sim k^2/q^6V$ and $\sim k^4/q^8V$ for fixed and free ends, respectively, and so we do not expect anomalous contributions from the power law tails. Below, we compute the excitation rate for

$$\begin{aligned}|i\mathbf{q}\cdot\mathbf{V}_{\mathbf{k}\lambda}(\mathbf{q})|^2 &= (2\pi)^3 k^2 \sum_{i=x,y,z}\delta(q_i-k_i) \\ &= (2\pi)^3\delta^{(3)}(\mathbf{q}-\mathbf{k})\ ,\end{aligned} \tag{4.16}$$

where $k_i = n_i\pi/L_i$, with n_i a positive or negative integer. Equation (4.16) corresponds to periodic boundary conditions in the same limit as the preceding two equations. Results for fixed or free surfaces (or combinations thereof) may be obtained by summing either different rates computed using Eq. (4.16) with appropriate substitutions for $\{k_i\}$ and dividing the result by 8.

We present results for either extremely relativistic or clustered Dirac neutrinos, taking the anisotropic of the distributions in the laboratory rest frame into account only where qualitatively important. For extremely relativistic neutrinos, we find

$$R^{(0)}_{\mathbf{k}l} \approx \frac{4\pi G_F^2 C_V^2 \rho n_\nu}{3\zeta(3)\mu^2 c_l}\int_{k/2T}^{\infty}\frac{dx\,x}{e^x+1}\ , \tag{4.17}$$

where we have also used the fact that $c_l \ll 1$ to simplify the remaining integral. For clustered neutrinos we find

$$R^{(0)}_{\mathbf{k}l} \approx \left(\frac{\pi}{8}\right)^{1/2}\frac{G_F^2 C_V^2 \rho\rho_\nu}{\mu^2\bar{p}c_l}\exp\left[-\frac{(k+m\mathbf{v}\cdot\hat{\mathbf{k}}+2mc_l)^2}{8\bar{p}^2}\right], \tag{4.18}$$

where $\bar{p} = m\sigma$; typically, $c_l \sim 10^{-5}$, so that $mc_l/\bar{p} = c_l/\sigma \ll 1$ can be neglected. In both cases, the excitation rates are approximately constant for $k \lesssim p_\nu$ and cut off rapidly, $k \gtrsim p_\nu$; in no sense may we regard the excitation rates as "coherent" since they do not depend on the volume of the solid. Moreover, the rates per mode are pitifully small: Their peak values are

$$\lim_{|\mathbf{k}|\to 0} R_{\mathbf{k}l} \approx \begin{cases} 1.3\times 10^{-37}\ \mathrm{s}^{-1} C_V^2\rho/\mu^2 c_{l,5} & \text{(relativistic)}\ , \\ 1.9\times 10^{-29}\ \mathrm{s}^{-1} C_V^2\rho\rho_{\nu,0.01}/\mu^2 c_{l,5} m_{10}\sigma_{-3} & \text{(clustered Dirac)}\ , \end{cases} \tag{4.19}$$

where $c_l = 10^{-5}c_{l,5}$ and $m = 10m_{10}$ eV. In a large solid, the number of modes susceptible to excitation could be substantial, approximately $p_\nu^3 V/6\pi^2$ or $\sim 10^7 V$ (m^3) for relativistic neutrinos and $\sim 2\times 10^{12}(m_{10}\sigma_{-3})^3 V$ (m^3) for clustered neutrinos. Even so, the expected rate of excitation of modes from the ground state is miniscule.

Usually, a target solid will not be in its ground state and there will be $N_{\mathbf{k}\lambda}$ phonons in a particular mode of the unperturbed system. The excitation rate for $(\mathbf{k}\lambda)$ is $\propto 1 + N_{\mathbf{k}\lambda}$, raising the possibility of considerable enhancement above $R^{(0)}_{\mathbf{k}\lambda}$ for modes "pumped" to large $N_{\mathbf{k}\lambda}$. However, interactions of the solid with background neutrinos may destroy phonons as well as create them, and the net reaction rate is the difference between the rates of upward and downward changes in $N_{\mathbf{k}\lambda}$. It is easy to show that for a laboratory solid moving through the neutrino sea at a velocity $\mathbf{v}$, the net rate of single-phonon production is

$$R_{\mathbf{k}\lambda} = R^{(0)}_{\mathbf{k}\lambda}\{1 - N_{\mathbf{k}\lambda}[\exp(\omega'_{\mathbf{k}\lambda}/T) - 1]\} \tag{4.20}$$

for extremely relativistic neutrinos and

$$R_{\mathbf{k}\lambda} = R^{(0)}_{\mathbf{k}\lambda}\{1 - N_{\mathbf{k}\lambda}[\exp(\omega'_{\mathbf{k}\lambda}/m\sigma^2) - 1]\} \tag{4.21}$$

for clustered Dirac neutrinos, where

$$\omega'_{\mathbf{k}\lambda} = \omega_{\mathbf{k}\lambda} + \mathbf{k}\cdot\mathbf{v} \tag{4.22}$$

is the excitation energy in the frame where the neutrinos are isotropic. For $|\mathbf{v}| \sim 10^{-3}$ and $c_1 \sim 10^{-5}$, $|\mathbf{k}\cdot\mathbf{v}| > \omega_{\mathbf{k}\lambda}$, and $\omega'_{\mathbf{k}\lambda}$ may be positive or negative; if the latter is true, $R_{\mathbf{k}\lambda} > 0$ (phonon production dominates), and if the former is true, $R_{\mathbf{k}\lambda} < 0$ (phonon destruction dominates). For extremely relativistic neutrinos, however, $|\mathbf{k}\cdot\mathbf{v}|/T \sim 10^{-3}$ and $|R_{\mathbf{k}\lambda}|$ only exceeds $R^{(0)}_{\mathbf{k}\lambda}$ substantially if $N_{\mathbf{k}\lambda} \gtrsim |\mathbf{v}|^{-1} \sim 10^3$. For clustered Dirac neutrinos, $|\mathbf{k}\cdot\mathbf{v}| \sim m\sigma^2$ and $|R_{\mathbf{k}\lambda}|/R^{(0)}_{\mathbf{k}\lambda} \sim N_{\mathbf{k}\lambda}$ in general. If $N_{\mathbf{k}\lambda}$ is large for many different modes, then the net rate of phonon production could be significantly increased over the ground-state excitation rate.

V. CONCLUSIONS

In this paper, we have examined a variety of different mechanical effects of cosmological neutrinos in some detail. We began by reconsidering the acceleration of individual target masses by neutrinos, a problem that has been treated elsewhere, both correctly and incorrectly. Our calculations corroborate the claim of previous investigators that the lowest-order steady forces on a target mass are $O(G_F^2)$, in spite of the fact that incident neutrinos are deflected by a potential $\propto G_F$ upon entering and exiting the target. We have demonstrated that this result is really not intrinsically quantum mechanical in nature by showing that it also follows from a purely classical calculation of the behavior of a target system bombarded by low-energy neutrinos.

Because the neutrino background density is only uniform on average, a target mass experiences fluctuating forces which may be larger than the steady forces it feels. If the steady force is $\mathbf{F}$ and the fluctuations are governed by a diffusion coefficient dp^2/dt, then the cumulative impulse due to steady forces will exceed the accumulated impulse due to fluctuations by a ratio S/N only after a time $(S/N)^2 t_c$ has elapsed, where $t_c = |\mathbf{F}|^{-2} dp^2/dt$. The required time scale for separating steady accelerations from velocity fluctuations due to the neutrino background may be surprisingly long; for example, for a spherical target of optimal size ($R \sim p_\nu^{-1}$), $t_c \sim$months for clustered Dirac neutrinos (or clustered Majorana neutrinos scattering from polarized targets) and $t_c \sim 10^7$ yr for extremely relativistic neutrinos. Even if all other sources of noise can be eliminated from an experiment designed to measure accelerations due to the neutrino background, these fluctuating forces due to the background itself must remain. It may be that the fluctuating accelerations themselves can be distinguished from other sources of noise since the fluctuation tensor $d(p_i p_j)/dt$ is generally anisotropic, with a preferred axis along the peculiar velocity of the Earth through the background. If so, it may be possible to exploit the fluctuations themselves in an experiment to detect cosmological neutrinos mechanically. However, this continuous description of the motion of a target mass in the cosmological neutrino background must be used carefully. As we have shown, the rate at which cosmological neutrinos are scattered by targets of size $\hat{R} \sim 1$ only exceeds t_c^{-1} by a factor of 10 or so. (See Table III.) The perturbation felt by a massive probe is impulsive, and only when a large number of bumps has occurred will the actual displacement converge to its expected value. Practically speaking, this requires the use of fairly large target masses, with radii $\hat{R}$ considerably larger than one, in order to guarantee substantial scattering rates, say, of order one per day. Unfortunately, the larger the target mass, the smaller its expected displacement, since $\mathbf{a} \sim \hat{R}^{-1}\ln(\hat{R})$ and $dv^2/dt \sim \hat{R}^{-4}\ln(\hat{R})$.

Some of the new experimental difficulties posed by fluctuating forces may be less severe for nonspherical targets. Although we have only studied spherical detectors in detail in this paper, we expect that the results remain qualitatively the same for nonspherical targets whose dimensions are roughly comparable in any direction. However, from our limited exploration of slab geometry in Sec. II E, it appears that $t_c \sim A^{-1}$ for targets with large surface area A in a plane, but modest thickness $L_3 \ll \sqrt{A}$ perpendicular to that plane; moreover, the target acceleration is independent of A. Thus one may not have to sacrifice acceleration to get acceptable t_c for slab targets, in sharp contrast to the situation for spherical detector masses.

Neutrino background density fluctuations are correlated in time and space, so that the accelerations felt by a pair of nearby targets are not independent of one another. Perhaps more interesting from a qualitative viewpoint is that the distortion of incident neutrino wave functions by one target can result in a nonzero acceleration of its neighbor, so that the pair of targets creates a mutual shadowing force. The range of the force is only $\sim p_\nu^{-1}$, and although its effective potential is $\propto 1/r$ at small separations, the shadowing interaction is far weaker than gravity. Ideally, its presence could be uncovered as a composition and separation dependence of the Newtonian coupling constant G. In practice, the effects are well below the accuracy of state of the art Cavendish experiment [24]. Slab geometry offers no new hope for detecting shadowing forces, which remain far weaker than gravity and short range for nonspherical targets.

Finally, we have moved upward in complexity from a two-body system to a many-body system and calculated the rates of excitation for normal modes of an atomic lattice (in the continuum limit). Although it may have been expected that the excitation of internal modes would be coherent, we found that in fact the rates per mode are independent of the volume of the solid. The total rates of excitation from the ground state, summed over modes for a reasonable target size, are so small that we can be confident that such excitations will never be detected: For a volume of order 1 m^3, the total rate of excitation by clustered Dirac neutrinos is only about one per Hubble time. The corresponding rate for relativistic neutrinos is considerably smaller. For solids with a range of normal modes "pumped" to large occupation numbers, the net rate of phonon production (or destruction) may be considerably larger, but to achieve rates as large as one per year would require large numbers of modes to have large occupation numbers (e.g., $\sim 10^{10}$ phonons in each of $\sim 10^{12}$ modes for excitation by neutrinos clustered in the galaxy).

There are a number of interesting issues which we have

not addressed here. One is the suggestion that photoemission from electrons in a metal coherently scattering cosmological neutrinos could be detectable [25]. In view of the results of our simpler evaluation of the excitation rate of normal modes of an atomic solid, we are skeptical that any coherent effects are actually possible and expect that a detailed calculation that includes the response of the metal properly would give results below even the most pessimistic estimates of the photoemissivity triggered by background neutrinos [26]. We have only computed the weak interactions of neutrinos with material targets and have not explicitly considered the possibility that neutrinos possess anomalous magnetic moments which can enhance their low-energy couplings substantially [25].

Most importantly, perhaps, we have not discussed at all whether or not there could be general arguments that the tiny mechanical effects derived in this paper cannot be detected in principle. To get an idea of the magnitude of the difficulty of detecting cosmological neutrinos, let us compare the expected motions of targets of various masses M with the standard quantum limit [27] $\Delta x_{\rm SQL}(t) = \sqrt{t/2M}$ on the observation of displacements in a time interval t. From the results of Sec. II, we find

$$\left(\frac{\langle|\mathbf{x}(t)|\rangle}{\Delta x_{\rm SQL}(t)}\right)^2 = M|\mathbf{a}|^2 t_c^3 \left[\left(\frac{t}{t_c}\right)^3 + \frac{2}{3}\left(\frac{t}{t_c}\right)^2\right] . \quad (5.1)$$

For Dirac neutrinos,

$$M|\mathbf{a}|^2 t_c^3 = \frac{4\pi\mu^2 E_\nu^9 v_\nu^{12}}{3G_F^2 C_V^2 \rho^3 n_\nu |\mathbf{v}|^4} \frac{\hat{R}^3 \mathcal{G}_D^3(\hat{R})}{\mathcal{F}_D^4(\hat{R})} , \quad (5.2)$$

where the dimensionless functions $\mathcal{G}_D(\hat{R})$ and $\mathcal{F}_D(\hat{R})$ were defined in Sec. II; from the various limiting results for these dimensionless functions given in that section, it is straightforward to show that $M|\mathbf{a}|^2 t_c^3$ is a decreasing function of $\hat{R}$. Numerically,

$$\frac{4\pi\mu^2 E_\nu^9 v_\nu^{12}}{3G_F^2 C_V^2 \rho^3 n_\nu |\mathbf{v}|^4} \approx \begin{cases} 5\times 10^{-3}\mu^2/C_V^2\rho^3 v_{-3}^4 \ \text{(extremely relativistic)} , \\ 0.3\mu^2 m_{10}^{10}\sigma_{-3}^8/C_V^2\rho^3\rho_{\nu,0.01} \ \text{(clustered Dirac)} , \end{cases} \quad (5.3)$$

where the various symbols have the same meanings as throughout the paper: ρ and μ are the mass density (here in units of g cm^{-3}) and mass per atom of the target and C_V is given by Eq. (2.27); for unclustered neutrinos, $\mathbf{v}$ is the velocity of the solar system through the neutrino background and $v_{-3} = 10^3|v|$; for clustered Dirac neutrinos, m_{10} is the neutrino mass in units of 10 eV, σ_{-3} is the velocity dispersion in units of $10^{-3}c$, and $\rho_{\nu,0.01}$ is the local halo mass density in units of $0.01 M_\odot$ pc^{-3}. [Naturally, these units have been chosen so that all of the parameters appearing in Eq. (5.3) are typically, or, in the case of Dirac neutrinos clustered in the Galaxy, hypothetically, of order unity.] If $t_{\rm SQL}$ is defined to be the value of t at which $\langle|\mathbf{x}(t)|\rangle/\Delta x_{\rm SQL}(t) \equiv 1$, then since Eq. (5.3) implies that $M|\mathbf{a}|^2 t_c^3 < 1$ for $\hat{R} \sim 1$ in each case (and $\ll 1$ for large targets, $\hat{R} \gtrsim 1$, for which $t_{\rm SQL}$ is smallest), we find that, for $\hat{R} \gtrsim 1$, $t_{\rm SQL} \approx (M|\mathbf{a}|^2)^{-1/3}$, which is a decreasing function of $\hat{R}$. For Dirac neutrinos clustered in the galaxy, we find that for $\hat{R} = 10^4$, which is equivalent to $R = 20 m_{10}^{-1}\sigma_{-3}^{-1}$ cm, $t_{\rm SQL} \approx 0.8 m_{10}^{5/3}\sigma_{-3}^{5/3}\mu^{4/3}/C_V^{4/3}\rho\rho_{\nu,0.01}^{2/3}$ years; for large $\hat{R}$, $t_{\rm SQL} \propto \hat{R}^{-1/3}(\ln\hat{R})^{-2/3}$. Although $t_{\rm SQL}$ may be only of order years for clustered Dirac neutrinos, the values of $t_{\rm SQL}$ for detection of extremely relativistic Dirac neutrinos are typically much longer: For $\hat{R} = 10^3$, which is equivalent to $T = 1.2$ m, $t_{\rm SQL} \approx 0.8\times 10^6 \mu^{4/3}/C_V^{4/3}\rho v_{-3}^{2/3}$ yr, and for large $\hat{R}$, $t_{\rm SQL} \propto \hat{R}^{-1/3}(\ln\hat{R})^{-2/3}$, which decreases so slowly with increasing $\hat{R}$ that $t_{\rm SQL} \gg$ years for any practically attainable values of $\hat{R}$. Of course, experimental detection schemes that rely on quantum nondemolition (QND) observations could be far more sensitive. However, standard estimates of the accuracy of QND experiments designed to measure weak classical forces do not strictly apply to the observation of mechanical effects of cosmological neutrinos [28]. This is because the interaction of the neutrino background with a target cannot be modeled as a continuous, classical force, since it involves stochastic and perhaps large deflections of individual quanta, in stark contrast with the interaction of a many-graviton gravitational wave with a massive probe.

ACKNOWLEDGMENTS

This research was supported in part by NSF Grant No. AST 91-19475. We thank K. Gottfried for useful conversations on some aspects of this work.

APPENDIX: DENSITY FLUCTUATION SPECTRUM [29]

Define the density fluctuation operator for plane wave states to be

$$\delta\hat{n}(x) = \frac{1}{V}\sum_{\mathbf{k}\neq\mathbf{k}'} \hat{a}_{\mathbf{k}}^\dagger \hat{a}_{\mathbf{k}'} e^{i(k-k')\cdot x} , \quad (A1)$$

where $x = (\mathbf{x}, t)$ and $k = (\mathbf{k}, \omega_{\mathbf{k}})$ and the dot product is of the four-vectors x and k, using normalization inside a box of volume V. The correlation function of density fluctuations is the expectation value of the operator

$$\hat{C}(x_1, x_2) = \tfrac{1}{2}[\hat{C}_a(x_1, x_2) + \hat{C}_a(x_2, x_1)] , \quad (A2)$$

where the unsymmetrized density fluctuation operator is

$$\hat{C}_a(x_1, x_2) = \delta\hat{n}(x_1)\delta\hat{n}(x_2) . \quad (A3)$$

[It is $\hat{C}_a(x_1,x_2)$ rather than $\hat{C}(x_1,x_2)$ that actually appears in scattering problems.] For a homogeneous, time-translation-invariant gas, we find

$$n_a^2(x) = \langle \hat{C}_a(x_1, x_1+x)\rangle = \frac{1}{V^2}\sum_{\mathbf{k}\neq\mathbf{k}'} N_{\mathbf{k}}(1-N_{\mathbf{k}'})e^{i(k-k')\cdot x} , \quad \text{(A4)}$$

where $\langle\,\rangle$ is evaluated in the neutrino background. Define the fluctuation spectrum by

$$n_a^2(x) = \int d^4q\, e^{iq\cdot x}\tilde{n}_a^2(q) ; \quad \text{(A5)}$$

combining the continuum version of Eq. (A4) with (A5) gives

$$\tilde{n}_a^2(q) = \int \frac{d^3k}{(2\pi)^3}\frac{d^3k'}{(2\pi)^3} N_{\mathbf{k}}(1-N_{\mathbf{k}'})\delta^{(4)}(k-k'-q) . \quad \text{(A6)}$$

For extremely relativistic neutrinos with $N_{\mathbf{k}} = (e^{k/T}+1)^{-1}$, Eq. (A6) gives

$$\tilde{n}_a^2(\mathbf{q},\sigma) = \frac{\Theta(q-|\sigma|)}{(2\pi)^5 q}\int_{(q+\sigma)/2}^{\infty} \frac{dp\, p(p-\sigma)e^{(p-\sigma)/T}}{(e^{p/T}+1)[e^{(p-\sigma)/T}+1]} . \quad \text{(A7)}$$

For clustered neutrinos with $N_{\mathbf{k}} = N_0\exp[-|\mathbf{p}-\mathbf{p}_0|^2/2\bar{p}^2]$, Eq. (A6) gives

$$\tilde{n}_a^2(\mathbf{q},\sigma) = \frac{\rho_\nu}{(2\pi)^{7/2}q\bar{p}}\exp\left[-\frac{(q/2-\mathbf{p}_0\cdot\hat{\mathbf{q}}+m\sigma/q)^2}{2\bar{p}^2}\right] , \quad \text{(A8)}$$

where ρ_ν is the neutrino mass density. In deriving Eq. (A8), we have neglected the "correction for Fermi suppression." Integrating Eq. (A8) over σ gives $n_\nu/(2\pi)^3$, which in turn implies the equal-time spatial correlation function $n_\nu\delta^{(3)}(\mathbf{x}_1-\mathbf{x}_2)$.

[1] See, for example, P. J. E. Peebles, *Principles of Physical Cosmology* (Princeton University Press, Princeton, 1993) or E. W. Kolb and M. S. Turner, *The Early Universe* (Addison-Wesley, Reading, MA, 1990) for reviews of big band cosmology.

[2] R. Opher, Astron. Astrophys. **37**, 135 (1974).

[3] R. R. Lewis, Phys. Rev. D **21**, 663 (1980).

[4] R. Opher, Astron. Astrophys. **108**, 1 (1982).

[5] P. Langacker, J. P. Leveille, and J. Sheiman, Phys. Rev. D **27**, 1228 (1983).

[6] N. Cabibbo and L. Maiani, Phys. Lett. **114B**, 115 (1982).

[7] P. F. Smith and J. D. Lewin, Phys. Lett. **127A**, 185 (1983).

[8] R. Opher, Astrophys. J. **282**, 398 (1984).

[9] J. D. Lewin and P. F. Smith, Astrophys. Lett. **24**, 59 (1984).

[10] P. F. Smith and J. D. Lewin, Astrophys. J. **318**, 738 (1987).

[11] P. F. Smith, Ann. N.Y. Acad. Sci. **647**, 425 (1991); see especially Sec. 3.5. See also P. F. Smith and J. D. Lewin, Acta Phys. Pol. B **15**, 1201 (1984); **16**, 837 (1985).

[12] For detailed reviews of neutrino cosmology, see Peebles [1] and Kolb and Turner [1]. Note that the momentum distribution of unclustered neutrinos remains frozen after neutrinos decouple at a temperature ~ 1 MeV whether or not the neutrinos are massive, and so in either case the characteristic neutrino momentum is presently $T \approx 1.95$ K, a factor of $(4/11)^{1/3}$ below the temperature of the cosmic microwave background, $T \approx 2.73$ K [see J. C. Mather *et al.*, Astrophys. J. **420**, 439 (1994)].

[13] This cancellation was also discussed more generally by Langacker *et al.* in Ref. [5].

[14] It is easily shown that total reflection of cosmological neutrinos plays no role in the dynamics of spherical targets for which the Born approximation is valid. For such targets, we may confine our attention to $|1-\sqrt{Q}| \ll 1$.

[15] See G. F. Smoot *et al.*, Astrophys. J. Lett. **371**, L1 (1991); **396**, L1 (1992); for our purposes, the relevant velocity is relative to the solar system barycenter. We do not consider the annual variation in velocity due to the Earth's orbit.

[16] We use the same model Langrangian as Langacker *et al.* [5].

[17] See Refs. [5–9] and L. Wolfenstein, Phys. Rev. D **17**, 2369 (1978); **20**, 2634 (1979).

[18] Actually, omitting Fermi suppression is only valid for unclustered neutrinos with $m \gg T/v$ as long as $R \lesssim T^{-1}$. Our results are therefore uncertain by a factor of perhaps 2 for large targets in this case.

[19] For such large targets, the Born approximation fails, but the eikonal approximation may be used. See, for example, K. Gottfried, *Quantum Mechanics* (Benjamin, New York, 1966), Sec. 13.2; L. I. Schiff, *Quantum Mechanics* (McGraw-Hill, New York, 1968), Sec. 38; see also Langacker *et al.* [5].

[20] To obtain limiting results for a thin slab, we have taken $L_1 \to \infty$ and $L_2 \to \infty$ using $\lim_{L\to\infty}[\sin(qL/2)/(qL/2)]^2 = (2\pi/L)\delta(q)$. We are not being careful here about the validity of the Born approximation, which may fail for incident neutrinos moving nearly parallel to the 1,2 plane if L_1 and L_2 are large enough; see, e.g., Langacker, *et al.* [5].

[21] See, for example, N. W. Ashcroft and N. D. Mermin, *Solid State Physics* (Saunders, Orlando, 1976), Chaps. 1 and 22.

[22] See, for example, Ashcroft and Mermin [21], Appendix L, for periodic boundary conditions.

[23] See, for example, Ashcroft and Mermin [21], Chap. 22, and L. Landau and E. M. Lifshitz, *Theory of Elasticity* (Pergamon, Oxford, 1970), Secs. 10 and 23.

[24] Newton's gravity constant G is still only known to an accuracy of about a part in 10^5. See C. M. Will, *Theory and Experiment in Gravitational Physics* (Cambridge University Press, Cambridge, England, 1993), Sec. 8.2, and references therein.

[25] A. Loeb and G. D. Starkman, in *Neutrino 90*, Proceed-

ings of the 14th International Conference on Neutrino Physics and Astrophysics, Geneva, Switzerland, edited by J. Panam and K. Winter [Nucl. Phys. B (Proc. Suppl.) **19**, 241 (1991)].

[26] S. Bahcall and A. Gould, Phys. Rev. D **43**, 940 (1991).

[27] See, for example, V. B. Braginsky and F. Khalili, *Quantum Measurement* (Cambridge University Press, Cambridge, England, 1992), Chap. 1.

[28] See, for example, Braginsky and Khalili [27], Chap. 4, and V. B. Braginsky, V. I. Vorontsov, and K. S. Thorne, Science **209**, 547 (1980).

[29] This appendix is based on L. Landau and E. M. Lifshitz, *Statistical Physics* (Pergamon, Oxford, 1969), Sec. 120, and E. M. Lifshitz and L. P. Pitaevski, *Statistical Physics*, (Pergamon, Oxford, 1980), Pt. 2, Sec. 86.